BAMS Article

The NASA ACTIVATE Mission

Armin Sorooshian,[a,b] Leong Wai Siu,[b] Kayley Butler,[c] Michael A. Brunke,[b] Brian Cairns,[d] Seethala Chellappan,[e,f] Jingyi Chen,[g,h] Yonghoon Choi,[e,f] Ewan C. Crosbie,[e,f] Lauren Cutler,[b] Joshua P. DiGangi,[e] Glenn S. Diskin,[e] Richard A. Ferrare,[e] Johnathan W. Hair,[e] Chris A. Hostetler,[e] Simon Kirschler,[i,j] Mary M. Kleb,[e] Xiang-Yu Li,[g] Hongyu Liu,[e,k] Allison McComiskey,[l] Soodabeh Namdari,[a] David Painemal,[e,f] Joseph S. Schlosser,[e,m] Taylor Shingler,[e] Michael A. Shook,[e] Sam Silva,[n] Kenneth Sinclair,[d,o] William L. Smith Jr.,[e] Cassidy Soloff,[b] Snorre Stamnes,[e] Shuaiqi Tang,[g,p] Kenneth L. Thornhill,[e,f] Florian Tornow,[d,o] George Tselioudis,[d] Bastiaan Van Diedenhoven,[q] Christiane Voigt,[i,j] Holger Vömel,[l] Hailong Wang,[g] Edward L. Winstead,[e,f] Yike Xu,[b] Xubin Zeng,[b] Bo Zhang,[e,k] Luke Ziemba,[e] and Paquita Zuidema[r]

KEYWORDS:
Atmosphere;
Clouds;
Aerosols;
In situ atmospheric observations;
Remote sensing;
Aerosol indirect effect

ABSTRACT: The NASA Aerosol Cloud Meteorology Interactions over the Western Atlantic Experiment (ACTIVATE) conducted 162 joint flights with two aircraft over the northwest Atlantic to study aerosol–cloud interactions (ACIs), which represent the largest uncertainty in estimating total anthropogenic radiative forcing. The combination of a high-flying King Air and low-flying HU-25 Falcon, equipped with remote sensing and in situ instruments, characterized trace gases, aerosol particles, clouds, and meteorological variables with data collected nearly simultaneously below, within, and above marine boundary layer (MBL) clouds. Flights spanning warm and cold seasons across 3 years (2020–22) provided a broad range of conditions associated with aerosol particles, cloud properties (including particle size and phase), and meteorology, ideally suited for robust ACI calculations and assessing how well models simulate a wide range of MBL clouds from stratiform to cumulus. ACTIVATE data suggest that drivers of cloud droplet number concentration N_d, including aerosol particles and MBL dynamics, vary between winter and summer months with a stronger potential to convert aerosol particles into cloud droplets in winter. Models of varying complexity not only highlight some skills in simulating winter and summer cloud types but also identify challenges that still need to be addressed such as treatment of turbulence, wet scavenging, and mesoscale organization. Remote sensing advances range from new retrieval methods for N_d, cloud phase classification, vertically resolved aerosol and cloud condensation nuclei number concentration, and ocean surface wind speed. This work describes these scientific and technological advances along with efforts in outreach and open data science.

DOI: 10.1175/BAMS-D-24-0136.1
Corresponding author: Armin Sorooshian, armin@arizona.edu
Supplemental information related to this paper is available at the Journals Online website: https://doi.org/10.1175/BAMS-D-24-0136.s1.

Manuscript received 30 April 2024, in final form 16 May 2025, accepted 20 May 2025

SIGNIFICANCE STATEMENT: Depending on the number and type of aerosol particles there are in the air, the properties of cloud droplets can vary in number concentration, size, and lifetime, and this leads to varying effects of clouds on climate and weather. We took an ambitious approach to investigate aerosol–cloud interactions, which represent the largest uncertainty in estimating human impacts on climate change. The NASA ACTIVATE mission conducted 162 joint airborne flights over the northwest Atlantic with two spatially coordinated planes making measurements relevant to understanding clouds spanning the continuum from stratiform to cumulus clouds. Along with newfound knowledge of how clouds evolve and interact with aerosol particles, extensive technological advancements were made assisted by the carefully designed sampling strategy.

AFFILIATIONS: [a] Department of Chemical and Environmental Engineering, The University of Arizona, Tucson, Arizona; [b] Department of Hydrology and Atmospheric Sciences, The University of Arizona, Tucson, Arizona; [c] Department of Civil and Environmental Engineering, University of Southern California, Los Angeles, California; [d] NASA Goddard Institute for Space Studies, New York, New York; [e] NASA Langley Research Center, Hampton, Virginia; [f] Analytical Mechanics Associates, Hampton, Virginia; [g] Atmospheric, Climate, and Earth Sciences Division, Pacific Northwest National Laboratory, Richland, Washington; [h] School of Atmospheric Physics, Nanjing University of Information Science and Technology, Nanjing, China; [i] Institute of Atmospheric Physics, German Aerospace Center, Cologne, Germany; [j] Institute of Atmospheric Physics, University Mainz, Mainz, Germany; [k] National Institute of Aerospace, Hampton, Virginia; [l] NSF National Center for Atmospheric Research, Boulder, Colorado; [m] NASA Postdoctoral Program, NASA Langley Research Center, Hampton, Virginia; [n] Department of Earth Sciences, University of Southern California, Los Angeles, California; [o] Center for Climate Systems Research, Columbia University, New York, New York; [p] School of Atmospheric Sciences, Nanjing University, Nanjing, China; [q] SRON Netherlands Institute for Space Research, Leiden, Netherlands; [r] Rosenstiel School of Marine, Atmospheric and Earth Science, University of Miami, Miami, Florida

1. Introduction

Aerosol–cloud interactions (ACIs) represent the largest uncertainty in estimating total anthropogenic radiative forcing (Bellouin et al. 2020). Airborne instruments can unravel ACI details by measuring relevant geophysical variables in and around clouds with a level of accuracy and detail that cannot be achieved by surface or spaceborne remote sensing. Figure 1 shows selected ACI-focused airborne campaigns in different regions of the world, demonstrating that there are understudied areas. The subject of this work helps fill the gap over the northwest Atlantic. In a recent review examining the northwest Atlantic and U.S. East Coast (>700 publications and >50 field campaigns since the 1940s), ACI emerged as the least studied topic among several themes (Sorooshian et al. 2020). ACI research is challenging due partly to the difficulty in identifying causation between aerosol perturbations and cloud changes. While aerosol levels have decreased significantly in recent decades over the U.S. East Coast (Sorooshian et al. 2020 and references therein) and northwest Atlantic (Park et al. 2024 and references therein), cloud fraction and cloud liquid water path have not changed as there has been no increase in sunlight reaching the ocean surface (Park et al. 2024). The Coupled Model Intercomparison Project phase 6 (CMIP6) ensemble revealed that the northwest Atlantic exhibits an especially large intermodel spread and large deviation in average surface temperature relative to observations (Bock et al. 2020), motivating more accurate simulation of marine boundary layer (MBL) clouds in the region and better

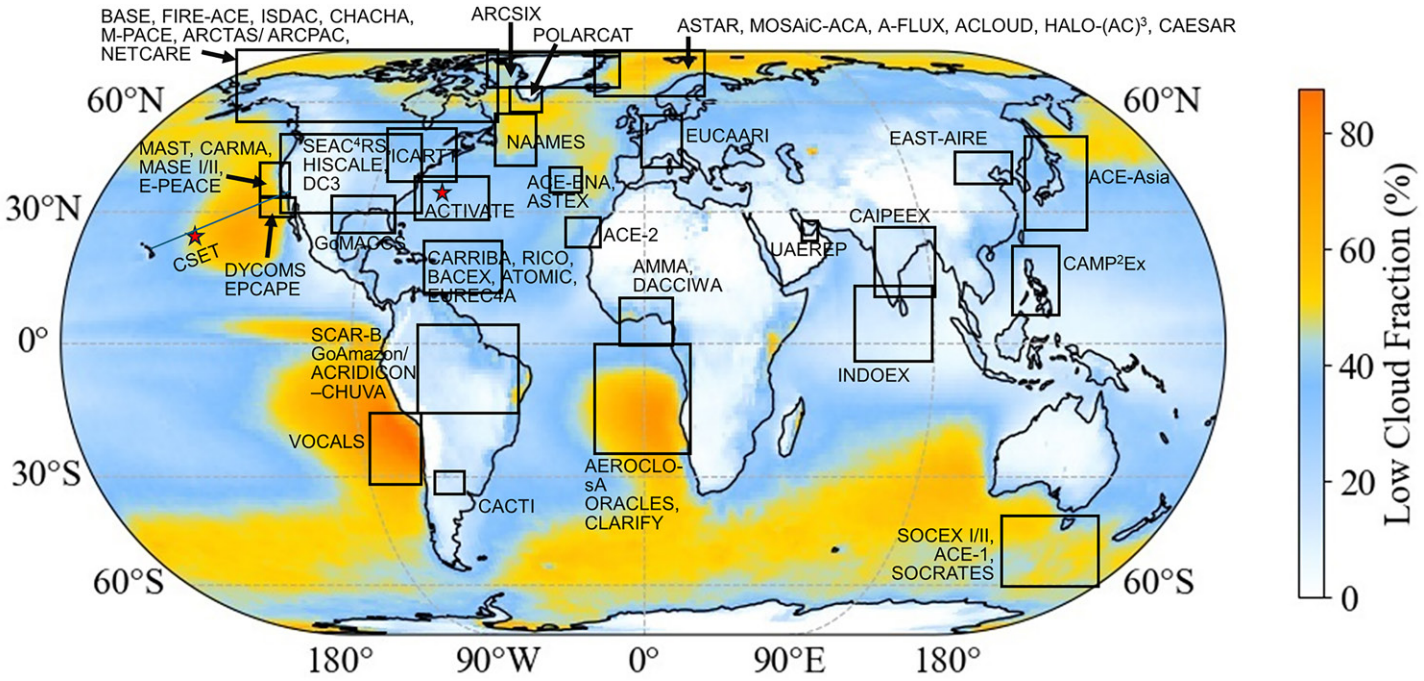

FIG. 1. A map summarizing locations of selected airborne campaigns that examined ACI. The boxes are meant to provide a general picture of the approximate area of campaigns with many stretching wide in spatial coverage such as those with aircraft capable of 8+ h of endurance. A red star is additionally provided to highlight ACTIVATE. The background coloring represents 3-yr mean (2020–22) values of low cloud fraction (pressure > 700 hPa) using the CERES Single Scanner Footprint (SSF) 1°-regional gridded monthly product based on *Aqua* MODIS data.

constraints on extratropical low cloud feedbacks (i.e., changes in low cloud with surface warming) that are largely responsible for climate sensitivity differences between CMIP5 and CMIP6 (Zelinka et al. 2020).

One of NASA's Earth Venture Suborbital-3 (EVS-3) missions, the Aerosol Cloud Meteorology Interactions over the Western Atlantic Experiment (ACTIVATE), tackled ACI with an extensive set of flights with two spatially coordinated aircraft over the northwest Atlantic across winter and summer seasons (2020–22). ACTIVATE responded to the National Academies of Science, Engineering, and Medicine Decadal Survey recommendation to study aerosols and clouds as one of the "most important" observing system priorities [National Academies of Sciences, Engineering, and Medicine (NASEM) 2018]. ACTIVATE's overarching objectives were to (i) study relationships between aerosol number concentration N_a, cloud condensation nuclei (CCN) concentration, and cloud droplet number concentration N_d to ultimately reduce uncertainty in model parameterizations of aerosol activation and cloud formation; (ii) improve process-level understanding and model representation of cloud properties and how they couple with cloud effects on aerosol; and (iii) assess remote sensing retrievals of aerosol and cloud properties related to ACI. This work shares what was learned and accomplished to date during ACTIVATE. Table S1 in the online supplemental material provides a nomenclature table to assist readers.

2. Overview of campaign execution

ACTIVATE flights were driven by the following strategies: (i) collect as much data as possible and facilitate easier data analysis by conducting flights in a routine and prescriptive manner where data can be easily combined and aggregated based on factors such as altitude relative to cloud and MBL top; (ii) use a coordinated aircraft approach with two aircraft synchronized in time and space to allow for near-simultaneous collection of remote sensing and in situ data in an atmospheric column from the surface to the height of the higher-flying aircraft (~9 km); and (iii) sample a wide range of aerosol, cloud, and

meteorological conditions, aided in part by flying in multiple seasons across three years: winter 2020 (22 flights, 14 February–12 March); summer 2020 (18 flights, 13 August–30 September); winter 2021 (21 flights, 27 January–2 April); summer 2021 (32 flights, 13 May–30 June); winter 2022 (55 flights, 30 November–29 March); and summer 2022 (31 flights, 3 May–18 June). Flights were conducted with NASA Langley's King Air (remote sensors and dropsondes) and HU-25 Falcon (in situ trace gas, aerosol, cloud, and state variables). Regarding (i)–(ii) above, more than 90% of the ~3–4-h joint flights (150 of 162 in total) involved "statistical surveys" where the King Air's main focus was flying at ~9 km above sea level in coordination with the lower-flying Falcon, which flew at different altitude legs (~3 min per leg) below, within, and above MBL clouds. The remaining 12 flights were called "process studies," involving more detailed plans at a specific focus area conducive to modeling studies such as the simulation of cold-air outbreaks (CAOs) and organized summertime cumulus clouds. The NASA Goddard Earth Observing System, version 5, Forward Processing (GEOS-FP; Rienecker et al. 2008; Molod et al. 2012; Lucchesi 2018) near-real-time 10-day weather prediction and forecasting of gases and aerosol particles guided the daily strategic planning of ACTIVATE research flights, especially on the selection of process study flights.

The aircraft were generally kept within close proximity during the 162 joint flights (within ~5 min and ~6 km for 73% of the time) (Schlosser et al. 2024). Flights targeted areas offering appreciable MBL cloud fraction while minimizing the influence from either cirrus clouds above the King Air altitude or obscuring midtropospheric layers that would affect remote sensing retrievals. Most flights were out-and-back flights based out of NASA Langley Research Center (LaRC) in Hampton, Virginia. ACTIVATE successfully remained on schedule with flights in the midst of the COVID-19 pandemic that started in the first deployment in February–March 2020. This was due in part to the use of smaller aircraft and locally based operations personnel with extraordinary skill and discipline. Very few people flew on the aircraft since individuals could operate multiple instruments as opposed to just one instrument. On a few occasions in 2022 when COVID-19 restrictions lessened, flights to secondary bases in New England and Bermuda extended the spatial range of the data. In the final month of the sixth deployment (June 2022), flights were exclusively conducted out of Bermuda to sample more of the remote marine atmosphere away from the influence of the U.S. East Coast and Gulf Stream (Fig. 2). Readers are referred to Sorooshian et al. (2023) for a much more detailed explanation of flight and instrument details.

A demonstration of the value of aircraft coordination is illustrated in Fig. 3 whereby the lidar operator on the King Air used observed lidar "curtains" of aerosol backscatter to provide real-time guidance to the Falcon pilots on the flight altitudes required to sample organic-rich biomass burning layers that are entraining into the MBL (see four vertically shaded areas of Fig. 3). The vertical characterization from the High Spectral Resolution lidar—generation 2 (HSRL-2) along with the in situ measurements on the Falcon shows the gradient in various gas and aerosol pollutants in the MBL. Above the mixing layer height, smoke layers stemming from sources over the central United States with different overall properties subside and/or advect horizontally at different speeds with the ability to alter MBL properties offshore over the remote ocean. Surface- and satellite-based datasets help show that biomass burning plumes, which, based on ACTIVATE data (Soloff et al. 2024), typically flow in the free troposphere and descend into the MBL and can interact with clouds over the northwest Atlantic with the ability to increase N_d and reduce droplet effective radius all else equal (Mardi et al. 2021). In addition to assessing remote sensing retrievals, these types of flight data open up opportunities to better understand the movement of marine atmospheric gradients offshore from polluted coastlines to remote marine areas like Bermuda (Soloff et al. 2024).

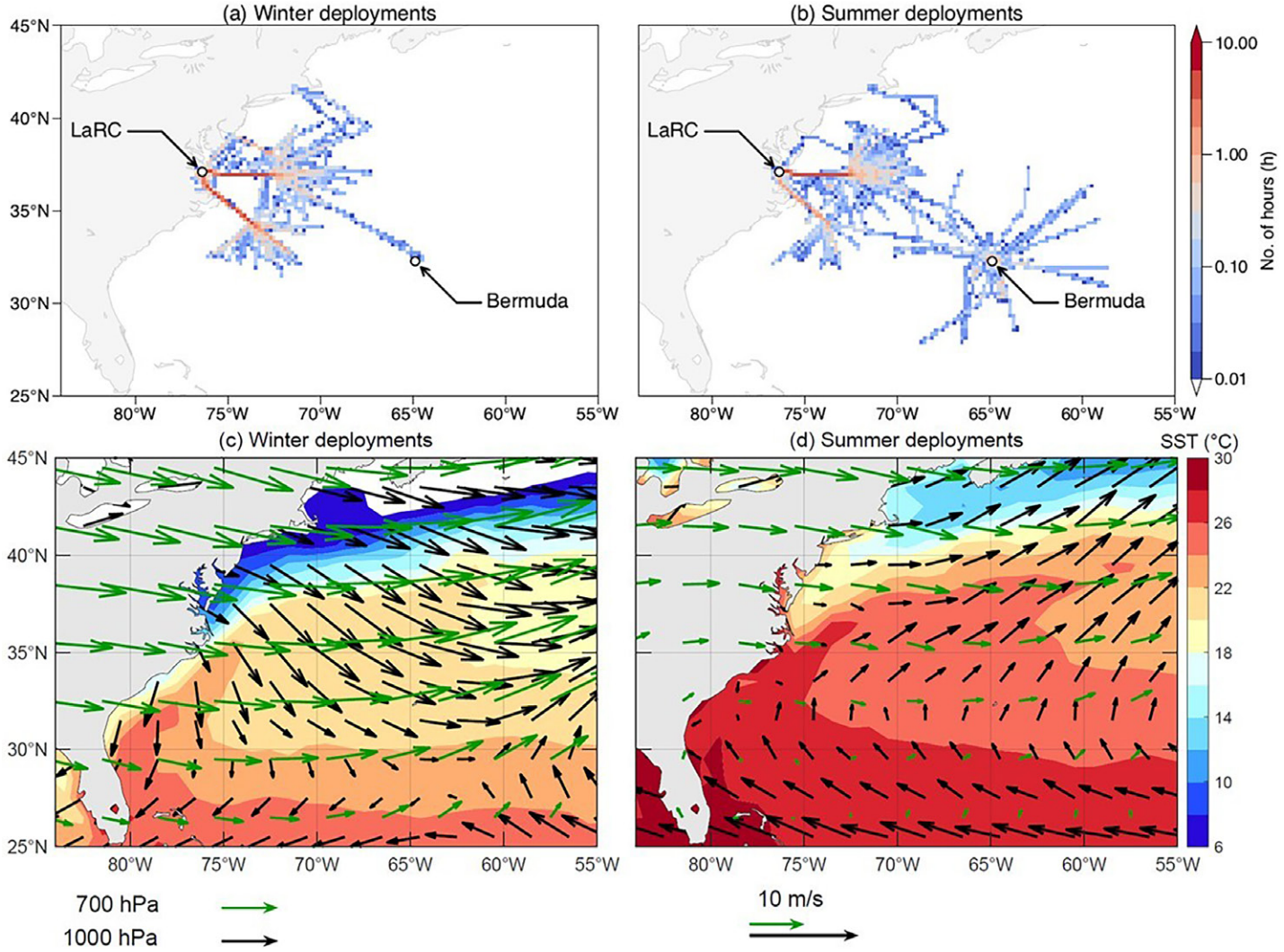

FIG. 2. (a),(b) ACTIVATE flight tracks colored by number of hours spent in individual 0.2° × 0.2° cells using 1-Hz data, which correspond to the HU-25 Falcon, but they are also representative of the King Air as the aircraft were usually spatially coordinated. The two climatological scenarios that govern the northwest Atlantic and that are used to group the ACTIVATE data into "winter" (November–April) and "summer" (May–September) deployments are illustrated. (c),(d) Mean MERRA-2, meteorological winds (arrows), and SST (colored contours) for winter and summer deployments. Near-surface (1000 hPa) and free tropospheric (700 hPa) winds are denoted by black and green arrows, respectively.

3. Conditions encountered during ACTIVATE

Atmospheric conditions for the northwest Atlantic are well documented in the literature (e.g., Angevine et al. 1996; Davis et al. 1997; Hurrell 1995; Lamb and Peppler 1987; Landsea and Franklin 2013). The northwest Atlantic atmospheric circulation is governed by two climatological features: (i) The Bermuda–Azores sea level pressure high, reaching peak strength in the summer, yields an anticyclonic circulation in the MBL and southwesterly winds parallel to the U.S. coastline north of ~30°N, along with easterly winds in the subtropics (south of ~30°N; Fig. 2d, black arrows), and relatively modest westerly winds in the free troposphere (Fig. 2d, green arrows); and (ii) starting in the fall, the Icelandic low (north of ~45°N) strengthens, limiting the Bermuda–Azores high's expansion while further promoting westerly boundary layer winds between 30° and 40°N. These winds are periodically modulated by frontal passages followed by a northerly wind component and strong free tropospheric westerlies (Fig. 2d, black and green arrows, respectively). As a result, summer flights experienced more trans-Atlantic flow influence, whereas winter flights had stronger relative influence from North American outflow and advection of cold polar air masses. ACTIVATE witnessed these seasonal wind pattern shifts, primarily sampling a region across the Gulf Stream, an oceanic

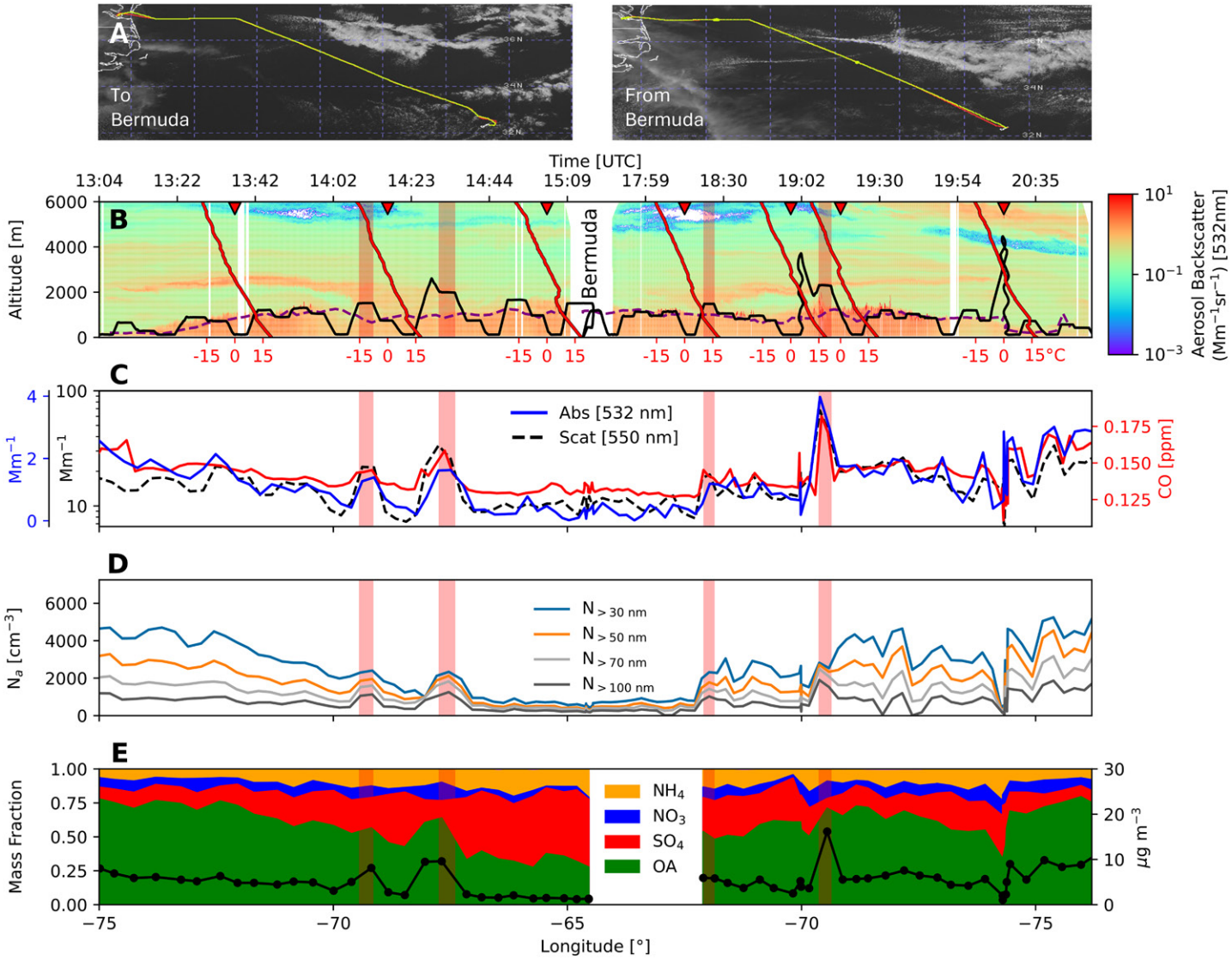

FIG. 3. An example from RFs 142–143 (22 Mar 2022) demonstrating how the spatially coordinated flight approach during ACTIVATE yielded important combined remote sensing and in situ data of an opportune smoke layer entraining into the MBL. These flights went from LaRC to Bermuda and back with refueling in between. (a) King Air (red) and HU-25 Falcon (yellow) flight tracks overlaid on *GOES-16* visible imager at (left) 14:01 and (right) 19:21 UTC. (b) HSRL-2 aerosol backscatter vertical distributions with locations of dropsondes launched from the King Air indicated by red arrows. The dropsonde temperature profiles are shown in red, with the horizontal positioning of the 0°C values on the *x* axis matching the dropsonde launch location arrows at the top of the panel. Aerosol mixing height is denoted by the dashed purple line, and the Falcon altitude is shown in black. The level legs which intersect the smoke layer are highlighted in red and displayed in subsequent panels. (c) Aerosol scattering and absorption coefficients (left *y* axis) and carbon monoxide (CO) (right *y* axis). (d) Aerosol number concentration above different dry diameters. (e) AMS mass fractions (left *y* axis) and total mass as a function of longitude (right *y* axis). The white gap in the middle indicates unavailable data. Aerosol data in (c)–(e) represent dry aerosol conditions, while those in (b) are at ambient conditions.

region featuring a strong sea surface temperature (SST) gradient (Fig. 2) and playing a key role in precipitation patterns due to pronounced surface fluxes (Minobe et al. 2008; Painemal et al. 2021; Seethala et al. 2021; Xu et al. 2022). Cloud fraction is highest in winter due to synoptic conditions favoring stratiform cloud decks on western edges of cyclones, whereas summertime has a lower cloud fraction due to the summer anticyclone promoting scattered shallow cumulus clouds. The 12 days chosen for the ACTIVATE process study flights proved to be ideal in hindsight as the synoptic meteorological conditions on those flights during winter (Li et al. 2023; Seethala et al. 2024; Tornow et al. 2022) and summer (Crosbie et al. 2024; Kirschler et al. 2022; Li et al. 2024a) were consistent with the seasonal climatology shown in Figs. 2c and 2d.

Liu et al. (2025) summarize the transport behavior of pollutants during ACTIVATE flights in different seasons. Flights in the wintertime coincided with the wake of cold front passages associated with midlatitude cyclones, with postfrontal transport in the MBL being a key mechanism for continental outflow. The aftermath of these cold fronts involved subsiding large-scale motion, which entrains air into the MBL, leading often to significant particle dilution (Tornow et al. 2022). Convection was important for vertical transport of pollutants especially in the southern flight area and more so in the summer.

Painemal et al. (2023) ingested daily 600-hPa geopotential heights and classified wintertime synoptic conditions into five characteristic regimes using a self-organizing map, a type of machine learning algorithm. That study emphasized a number of key points: (i) The dynamics of midlatitudinal clouds in the northwest Atlantic vary significantly from classical stratocumulus cloud regimes owing to much stronger surface forcing; (ii) dry and cold air promotes a jump in surface heat fluxes during CAOs, which coincide with a "trough regime" with high cloud fractions; and (iii) predominant winds during CAOs (offshore) explain the maximum in N_d in the trough regime. Clustering techniques such as self-organizing maps have benefits for ACI studies since traditional binning metrics [e.g., lower-tropospheric stability (LTS) and subsidence] are prone to covariance between smaller spatial-scale meteorological drivers and cannot account for the regional-scale factors that drive cloud variability. Regarding (i) above, traditional metrics such as LTS and the estimated inversion strength are not well related to lower cloud amount over the northwest Atlantic (Cutler et al. 2022); CAO index and surface forcing are better predictors (Painemal et al. 2023).

Figure 4 and Fig. S1 showcase the spectrum of weather, aerosol, and cloud conditions experienced across ACTIVATE's 179 flights (note 17 flights were with a single plane and 162 were joint), with seasonal statistics reported in Table S2. Figure 4 and Fig. S1 captions provide measurement details. A motivation for ACTIVATE was its distinctly different dynamical situation compared to subtropical stratocumulus regions (Sorooshian et al. 2019), which is

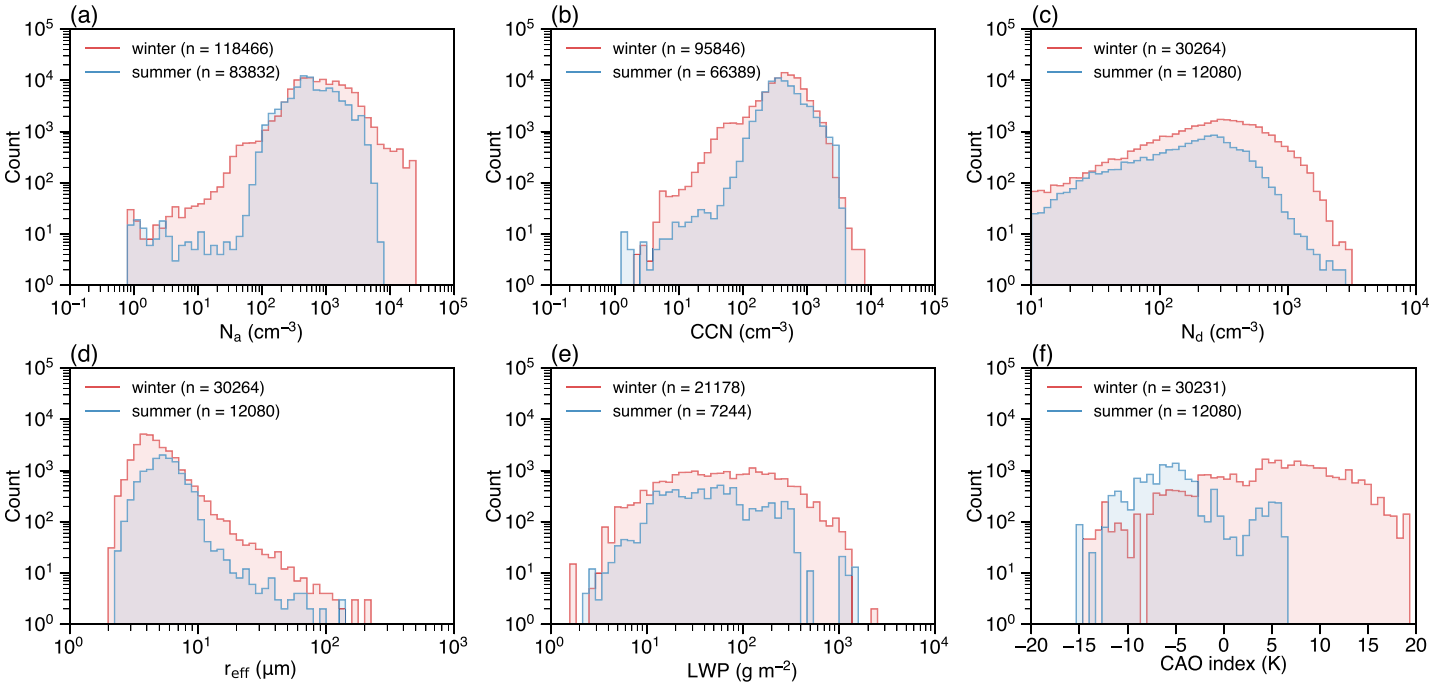

FIG. 4. Histograms showing the range of conditions encountered during ACTIVATE flights, with in situ results based on 1-Hz data from the Falcon. (a) Aerosol number concentration N_a from the combination of a scanning mobility particle sizer (SMPS) and laser aerosol spectrometer (LAS) (particle diameter range: 0.01–5 μm), (b) CCN number concentration (supersaturation ~0.2%–0.7%) BCBs, (c) cloud droplet number concentration N_d above cloud base (ACB) from a combination of the FCDP and 2D-S: FCDP + 2D-S$_{horizontal\ arm}$ (3–1465 μm in diameter), (d) ACB values of droplet effective radius r_{eff} (FCDP + 2D-S$_{horizontal\ arm}$), (e) *GOES-16* values for LWP during periods coincident with the HU-25 Falcon ACB leg, and (f) ERA5 values of CAO index ($\theta_{SKT} - \theta_{850hPa}$).

evident from the lower values of LTS ($\theta_{700\text{hPa}} - \theta_{1000\text{hPa}}$: 25th/75th percentiles for winter and summer = 13.5/18.5 K and 13.3/18.2 K, respectively). Boundary layer cloud thicknesses H encompass values between 0.1 and 3 km, and liquid water paths (LWPs) reached up to 1550 g m^{-2}, while droplet effective radii r_{eff} had winter/summer medians of 4.4/5.4 μm. A microphysical link between aerosols and clouds is N_d, which reached up to ~2970 cm^{-3} in select flights [median values, though much lower, are also elevated in winter (275 cm^{-3}) vs summer (195 cm^{-3}]. CCN number concentration reached up to ~12 070 cm^{-3} (winter/summer median = 438/406 cm^{-3}). Since clean conditions are linked to ACI assessment differences between models and observations (e.g., Gryspeerdt et al. 2023), it is relevant to note the following percentages of the ACTIVATE dataset for which CCN concentration was below 100 cm^{-3}: 4.3% (cumulative), 6.5% (winter), and 1.0% (summer). The ranges for these key aerosol and cloud geophysical variables are in significant contrast with the U.S. West Coast where several airborne campaigns over the northeast Pacific found N_d reaching as high as only 400 cm^{-3}, cloud thickness up to 1150 m, and LWP as high as 310 g m^{-2} (Sorooshian et al. 2019).

4. ACTIVATE results toward objective 1: Aerosol, CCN, and N_d

a. Aerosol composition. Central to aerosol effects on clouds is a comprehensive picture of the northwest Atlantic's atmospheric composition profile. The predominant aerosol chemical profile over the northwest Atlantic is a mix of sulfate, organic, and sea salt (Dadashazar et al. 2022, 2021b; Liu et al. 2025) with episodic influence from dust and smoke, along with more favorable conditions for ammonium and aluminum salts in the wintertime with lower temperatures (Corral et al. 2022a). Anthropogenic emissions are most influential for aerosol optical depth (AOD) by the U.S. East Coast (70%–90%) and decrease toward the southeast (~20% by Bermuda), which is a pattern opposite to the relative contribution of marine emissions (Liu et al. 2025). During summer, biomass burning influences AOD more with substantial plumes arriving from western North America. The southeast United States is a significant source of agricultural burning and natural fires that can greatly enhance both CCN levels and trace gas levels over the northwest Atlantic, especially between October and May (Corral et al. 2020; Edwards et al. 2021). Although not a relatively large contributor to AOD across the northwest Atlantic except at times in summer between Bermuda and Florida, long-range transport of dust from different regions impacts the U.S. East Coast and northwest Atlantic at all times of the year (Aldhaif et al. 2020; Zuidema et al. 2019).

The continental outflow of aerosol in the MBL transitions from organic-rich nearshore to sulfate-rich farther offshore (e.g., Fig. 3) closer to areas such as Bermuda (Dadashazar et al. 2022; Soloff et al. 2024). Hilario et al. (2021) showed that aqueous processing promotes the production of both sulfate and organics. Organics in the free troposphere are influenced by biomass burning with an especially strong signature between 1.5 and 6.0 km in August–September 2020 owing to wildfires around the western United States (Liu et al. 2025). Nucleated particles with diameters between 3 and 10 nm were common throughout the ACTIVATE flights but especially in the wintertime and also more specifically above cloud tops coinciding with cold/dry air and low total aerosol surface area concentrations (Corral et al. 2022b).

Over the northwest Atlantic, sea salt contributes appreciably to AOD (Corral et al. 2021), to halogen chemistry (Edwards et al. 2024), to ACI as a prominent source of CCN (Liu et al. 2025), and to cloud water and rainwater ionic composition (Aldhaif et al. 2021; Corral et al. 2020, 2021; Gonzalez et al. 2022; Ma et al. 2021).

b. Aerosol particles as CCN and modulators of cloud microphysics. A traditional way of examining ACI is the usage of metrics relating cloud microphysical variables such as r_{eff},

cloud optical depth τ_c, and N_d to a subcloud aerosol proxy variable such as N_a (e.g., McComiskey et al. 2009) with implications for model parameterizations. ACTIVATE's high volume of sampling around clouds is leveraged in Fig. 5 to show such relationships. The ACI metric relating N_d to N_a, $d\ln N_d/d\ln N_a$, should range from 0 to 1 (e.g., Feingold et al. 2001) with winter and summer values being 0.51 and 0.57, respectively. For context, ACI values relating N_d to N_a from airborne studies in other regions range from 0.26 to 1 (McComiskey and Feingold 2008; Painemal and Zuidema 2013). ACI metric calculations can be sensitive to data analysis methods, and they can lose details associated with aerosol properties, updraft velocity, and processes such as cloud entrainment and drizzle (Duong et al. 2011; McComiskey and Feingold 2012; McComiskey et al. 2009).

Recent studies are highlighted to address features related to ACI that complement the results in Fig. 5. CCN concentrations (Soloff et al. 2024) and N_d (Dadashazar et al. 2021b; Painemal et al. 2021) exhibit a decreasing gradient offshore of the U.S. East Coast out toward as far as Bermuda. In the golden flights [research flight (RFs) 142–143] highlighted by Soloff et al. (2024) on 22 March 2022 when continental outflow was aligned with the Falcon path from Virginia to Bermuda, CCN (~0.37% supersaturation) levels in the MBL dropped from 3000 cm^{-3} nearshore to ~500 cm^{-3} by Bermuda. It is not uncommon for offshore N_d gradients to drop from >1000 to <100 cm^{-3} over a horizontal span of >100 km (Dadashazar et al. 2021b; Seethala et al. 2024). Wet scavenging was shown to be an important process leading to the removal of aerosol transported from the U.S. East Coast toward Bermuda (Dadashazar et al. 2021a).

The N_d values are highest in winter owing partly to more efficient conversion of particles to droplets assisted by stronger updraft velocities (Dadashazar et al. 2021b; Kirschler et al. 2022; Painemal et al. 2021; Seethala et al. 2024), although N_a tended to be higher on average in winter too (Table S2). Kirschler et al. (2022) additionally show that while dynamics (e.g., updraft velocity) more effectively explain N_d variations between seasons, aerosol size distributions affect N_d values more within a season. The strong surface fluxes over the northwest Atlantic during the winter (Seethala et al. 2021) not only promote stronger turbulence (Brunke et al. 2022) and efficient droplet activation (Dadashazar et al. 2021b; Kirschler et al. 2022) but also entrain dry free tropospheric air into the MBL yielding entrainment rates that are an

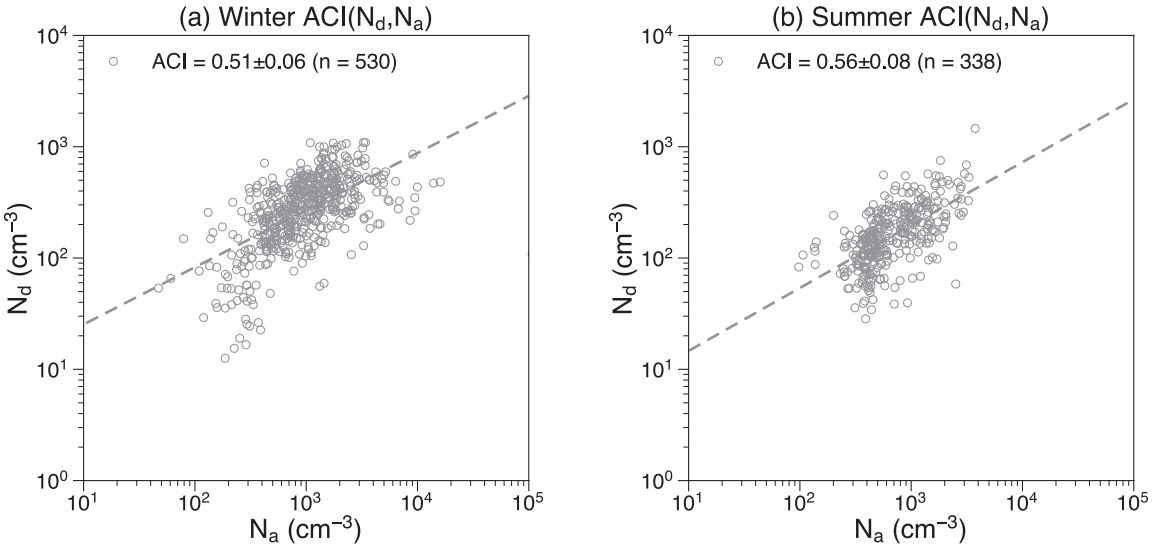

FIG. 5. ACI metric ($d\ln N_d/d\ln N_a$) values based on ACTIVATE Falcon leg mean values of in situ N_a and N_d measurements described in Fig. 4 for the (a) three winter and (b) three summer deployments, with the total number of data points in the panels and the ACI metrics represented as *n*. Aerosol data N_a from below cloud and cloud data N_d just ACB are compared using adjacent Falcon-level legs. Equation of the best fit and number of points *n* are shown along with a dashed one-to-one line.

order of magnitude larger than in subtropical stratocumulus regions (Tornow et al. 2022). This has the consequence of influencing MBL deepening (Chen et al. 2022; Painemal et al. 2023), occasionally resulting in cloudy MBL depths in excess of 2.5 km during CAOs (Seethala et al. 2024) with significant consequences for the MBL CCN budget (Tornow et al. 2022).

5. ACTIVATE results toward objective 2: Cloud characteristics

ACTIVATE focused on multiple seasons to collect in situ and remote sensing data across a range of cloud types driven by changes in atmospheric circulation and SST changes (Painemal et al. 2021). A statistical summary of ACTIVATE's cloud properties based on Falcon in situ wing-mounted optical probes, specifically the fast cloud droplet probe (FCDP) and two-dimensional stereo (2D-S), is provided by Kirschler et al. (2023). Below, we highlight selected observations relevant to each season.

a. Winter. In situ data confirm that the majority of MBL clouds sampled during winter flights possessed temperatures below 0°C (~61%) and were often, but not always, mixed phase or ice (~24%) (Kirschler et al. 2023). Altitude distributions of MBL clouds revealed a peak in winter at 1.3 km versus only 0.5 km in summer (Kirschler et al. 2023), which aligns with the trend in MODIS cloud-top heights (CTHs) (Painemal et al. 2021). In contrast to summer, the winter clouds exhibit generally higher N_d and lower effective droplet diameters for liquid clouds, suggestive of less efficient collision–coalescence and suppressed precipitation, with the precipitation typically expected farther downwind where satellite imagery confirms cloud regime transitions (e.g., Fig. 6a). Precipitation was more frequent in winter than summer, with mixed-phase cloud fraction and precipitation exhibiting both a latitudinal gradient with higher values to the north, especially north of 37.5°N (Kirschler et al. 2023), and a longitudinal gradient (Seethala et al. 2024). Vertical distributions of mixed-phase cloud properties show reductions in N_d and liquid water content (LWC) above 1.5 km in favor of increases in ice water content (IWC), ice number concentration N_{ice}, and effective diameter of ice, suggestive of glaciation, ice aggregation, and the Wegener–Bergeron–Findeisen processes (Kirschler et al. 2023 and references therein).

ACTIVATE's wintertime flights were conducive to gaining a deep understanding of CAOs coinciding with postfrontal systems of midlatitudinal storms, as 81 of 179 total flights were classified as having had such events (dates and criteria in Table S3). As cold air advects over the warm sea surface, a jump in surface heat fluxes can give rise to cloud streets. As the stratiform cloud deck deepens against a typically subsiding free troposphere and moves downwind, the overcast cloud deck increases in LWP, eventually inducing the formation of substantial rain that breaks up the cloud deck into a cloud field with reduced overall albedo (Seethala et al. 2024; Tornow et al. 2021). ACTIVATE studies show that this breakup point can be delayed with enhanced CCN concentrations while also being expedited with higher N_{ice} (Tornow et al. 2021). Prior to the breakup, CCN concentrations can be reduced significantly due to entrainment of low-CCN free tropospheric air, which is often associated with free tropospheric dry-air intrusion (Tornow et al. 2022). Tornow et al. (2023) additionally showed that meteorological patterns associated with dry-air intrusions from the upper troposphere can expedite transitions by enabling earlier formation of substantial rain closer to the low pressure center.

An archetypal CAO event sampled during a morning flight conducted on 18 January 2022 (RF 105) is depicted in Fig. 6. The *GOES-16* visible imagery (Fig. 6a) illustrates the eastward progression of the sampled cloud field, from clear air to overcast stratiform clouds and finally to broken cellular cumulus clouds. The initial sampling of clear air near the coast reveals N_a for particle sizes greater than 10 nm ranging from 600 to 800 cm^{-3}. The observed clouds were initially thin with cloud tops around 1.5 km (Fig. 6c). Farther east, the MBL progressively

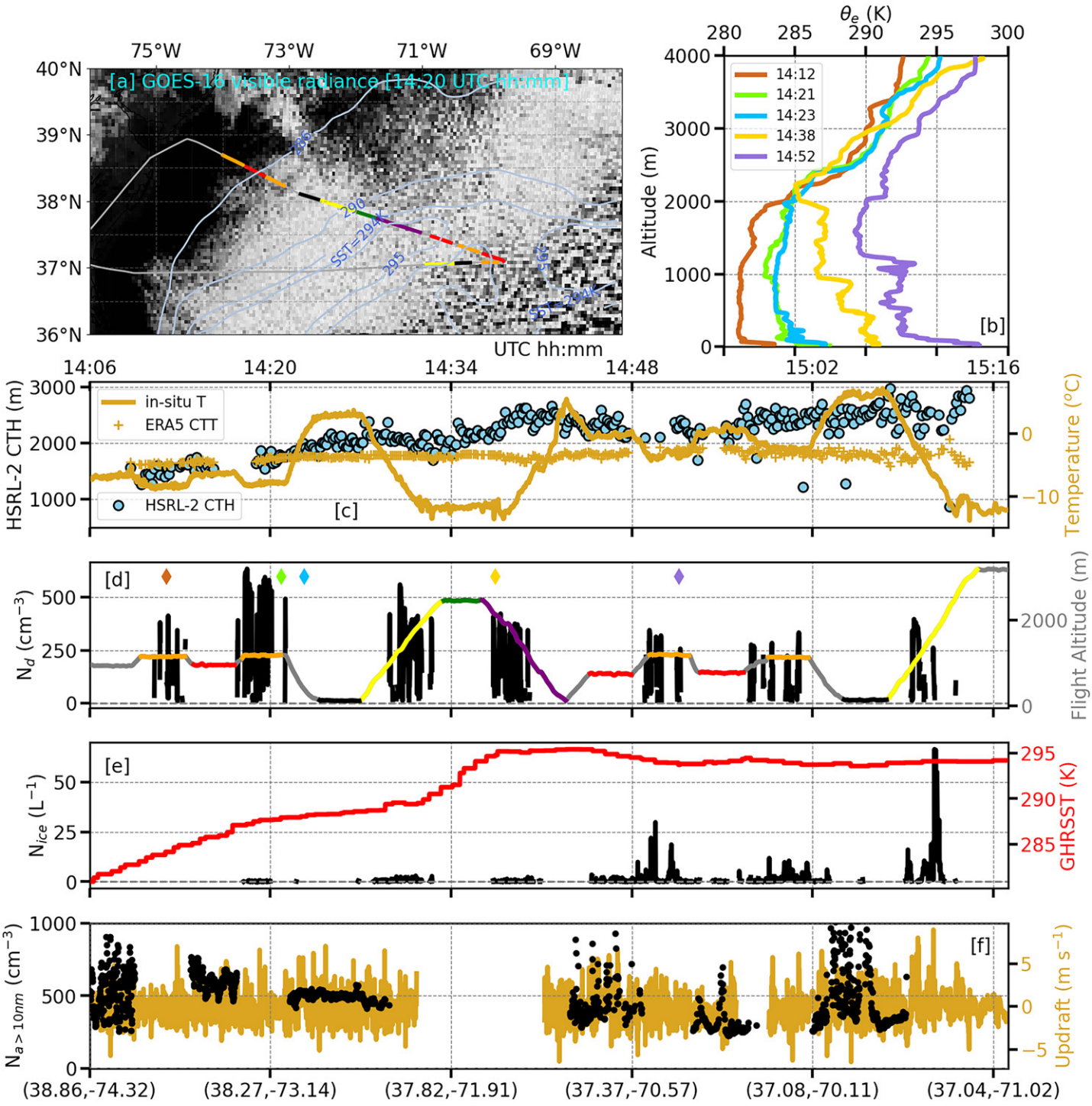

FIG. 6. CAO flight along the boundary layer flow on 18 Jan 2022 (morning flight; RF105): (a) *GOES-16* visible image with the flight tracks overlaid, with color-coded segments described in (d). (b) Profiles of equivalent potential temperature θ_e derived from dropsondes for the times indicated in the legend. (c) HSRL-2 measured CTH (blue circles; left *y* axis), in situ temperature from the Falcon, and cloud-top temperature ("x" symbol) derived from ERA5 temperature profile at the HSRL-2 CTH (right *y* axis). (d) The cloud droplet number concentration N_d from FCDP, and on the right *y* axis the Falcon flight track with color code representing the flight pattern as follows: ACB (orange), BCB (red), minimum altitude (MinAlt; black), above boundary layer (ABL; green), ascending/profiling (ascent; yellow), and descending/profiling (descent; purple). The colored diamonds at the top of the panel correspond to the respective dropsonde data with matching colors in (d). (e) The ice number concentration N_{ice} from 2D-S measurements and satellite-derived GHRSST (red; right *y* axis). (f) Falcon measurements of N_a derived from the LAS and the updraft velocity (orange; right *y* axis).

deepens (Fig. 6b), with cloud tops reaching heights up to 3 km (Fig. 6c, light blue circles) under a weak temperature inversion. Supercooled cloud droplets were observed throughout the flight, featuring an eastward reduction in N_d from around 600 to 250 cm^{-3} as the cloud

deepened, primarily due to the collision–coalescence process enhanced by strong updrafts (Figs. 6d,f), and likely modulated by cloud-top entrainment. Ice formation was detected early in the cloud development process, particularly during the second in-cloud leg (Fig. 6e), where the cloud temperatures were approximately −8°C, also reported in Seethala et al. (2024). This suggests the presence of ice-nucleating particles and evidence of a mixed-phase regime from the initial stage of cloud occurrence, when both supercooled water droplets and ice particles coexisted during the CAO event. The comparable concentration between N_d and particles larger than 10 nm suggests that a significant N_a fraction was activated into CCN. As the flight track reached the eastern edge, the cloud field began to break up, with N_{ice} exceeding 25 L^{-1}, preceding the transition into an open-cell structure. The second below-cloud-base (BCB) leg provided evidence of ice precipitation, predominantly graupel (as observed from 2D-S images; e.g., Seethala et al. 2024), just before the clouds transitioned to open-cell stratocumuli. During the inbound ascent leg, in the vicinity of the open-cell region (~70.5°W), N_{ice} exceeded 60 L^{-1} in regions with the strongest updrafts (up to 9 m s^{-1}). The features sampled during this specific flight are generally representative of those collected in CAO events (Seethala et al. 2024).

b. Summer. Strengthening of the Bermuda–Azores high in the summer promotes weaker surface fluxes and turbulence, accompanied by reduced LTS compared to winter, giving rise to shallow cumulus clouds with low spatial coverage (Painemal et al. 2021). This makes the ACTIVATE summertime data opportune for research because these clouds are underpredicted in terms of spatial coverage compared to observations (Painemal et al. 2021; Rémillard and Tselioudis 2015), and their response to warming accounts for large uncertainty in climate model cloud feedbacks (Bony and Dufresne 2005; Bretherton 2015; Sherwood et al. 2014).

In summer, process study flights were focused on prevalent regions of mesoscale organization observed in shallow cumuli and have been summarized by Crosbie et al. (2024). These cloud systems were observed over the Gulf Stream and in the region around Bermuda and are most commonly associated with the southwest flank of the Bermuda–Azores high, which advects moist tropical air masses into the region. Despite being located within the extratropics, the circulation pattern and the anomalously warm SSTs associated with the Gulf Stream make these cloud studies similar to conditions found deeper into the tropics. A particular motivation for these flights is the growing interest in the spatial distribution of shallow convection in relation to cloud radiative effects and the transition to deep convection as well as the ability of models to replicate mesoscale overturning circulations.

Crosbie et al. (2024) suggest that numerous factors control the vertical extent of cloud heights and spatial organization rather than just local thermodynamic drivers such as LTS and the moisture profile. Further, a "memory effect" could control how the cloud clusters evolve after formation rather than instantaneous factors such as the relationship to forcings like wind shear. Entrainment and detrainment and the scale of convective updrafts and downdrafts were critical to the cloud microphysical structure and evolution, and a notable observation was secondary droplet activation in the upper parts of the clouds. Future work is warranted to examine more deeply the role of aerosol particles in these process study cases and the broader dataset of summertime cumulus statistical surveys that are impacted by diverse aerosol sources such as African dust, continental pollution, biomass burning, and background marine particles.

6. ACTIVATE results toward objective 3: Remote sensing and technological advancement

The near-simultaneous and collocated collection of remote sensing and in situ data from ACTIVATE's two aircraft was crucial to evaluating existing and new aerosol and cloud remote sensing retrievals. An example relates to retrieving CCN concentrations, which is crucial for

determining the anthropogenic impacts on ACI (Stier 2016) but is challenging because remote sensing techniques operating in the visible part of the spectrum have reduced sensitivity to the size range of most CCN particles (diameter ~70–200 nm) (Andreae 2009). Attempts to infer CCN concentrations by extrapolating from remote sensing measurements have achieved only limited success (Andreae 2009; Gassó and Hegg 2003; Ghan and Collins 2004; Ghan et al. 2006; Kapustin et al. 2006; Shinozuka et al. 2015); a recently published method of retrieving CCN from Cloud–Aerosol Lidar with Orthogonal Polarization (CALIOP) profiles as part of the NASA *Cloud–Aerosol Lidar and Infrared Pathfinder Satellite Observations* (*CALIPSO*) satellite found uncertainties ranging between a factor of 2 and 3 (Choudhury and Tesche 2023). In contrast, much smaller uncertainties were found using a new machine learning (ML) methodology for retrieving vertically resolved CCN and aerosol absorption that was developed using remote sensing and in situ measurements from ACTIVATE and three other recent NASA field missions over the continental United States, southeast Atlantic Ocean, and over the Pacific Ocean near the Philippines (Redemann and Gao 2024). Airborne in situ CCN measurements were used to train advanced ML algorithms that used coincident HSRL-2 observations of aerosol backscatter and extinction to derive aerosol absorption and CCN. The ML model that used this full set of HSRL-2 and in situ data provided vertically resolved CCN (0.4% supersaturation) to within ±30% for 66% of the data and ±50% for 82% of the data. These percentages increased to 85% and 93%, respectively, when temperature and relative humidity from reanalyses were also used as predictors in the models.

Several advancements were made possible by the combinations of instruments used on a given aircraft along with the joint use of two aircraft. This is well illustrated by the combination of HSRL-2 and Research Scanning Polarimeter (RSP) measurements used to determine cloud-top N_d in warm clouds (Hair et al. 2024). HSRL-2 provided profiles of cloud-top extinction and average lidar ratios (i.e., cloud extinction/cloud backscatter) to 2.5 optical depths into the cloud, and RSP provided cloud drop size distribution derived from the cloud bow region of the scattering phase function. These measurements were combined to derive the cloud-top N_d. These lidar retrievals of cloud extinction and the retrievals of N_d from lidar combined with the RSP were generally in good agreement with the corresponding values derived from the airborne in situ measurements acquired near cloud top. Figure 7 shows a comparison of the

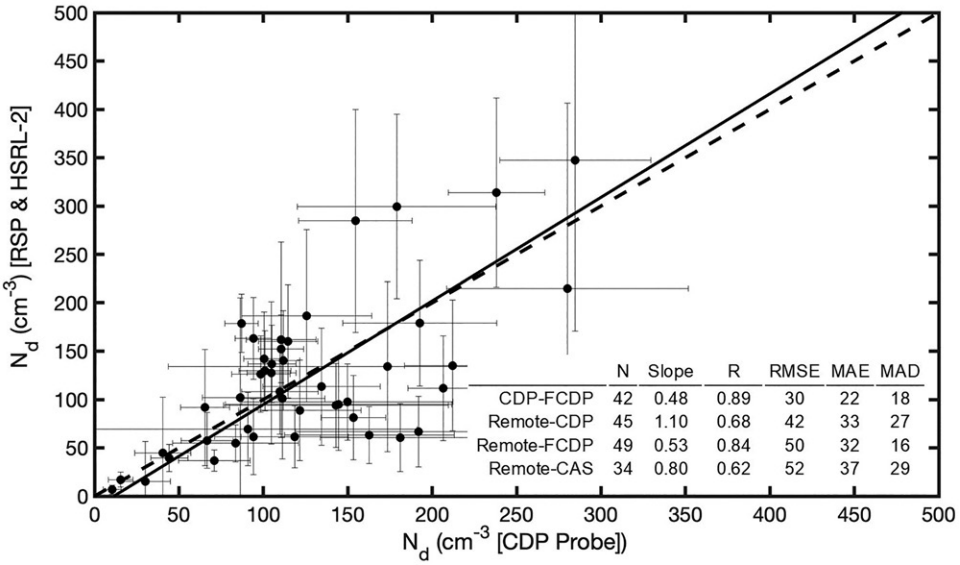

Fig. 7. Comparison of N_d measurements from the combined lidar and polarimeter retrieval (ordinate) to the CDP (abscissa) sampled during the cloud-top legs over the entire ACTIVATE dataset. Dashed line is 1:1 line. The inset table shows comparison metrics for the combined remote sensor retrievals from RSP and HSRL ("Remote") and the different wing-mounted cloud probes used: CDP, FCDP, and CAS. *N* = number of points; *R* = correlation coefficient; RMSE = root-mean-square error; MAE = mean absolute error.

remote sensing retrievals and in situ measurements of N_d from one such probe [cloud droplet probe (CDP)] with other comparisons shown in the inset table. Mean absolute deviations (MADs) between these remote sensing retrievals and in situ measurements were 16%–29% with correlation coefficients between 0.62 and 0.89.

A further advantage of the joint aircraft flight strategy was to evaluate the quantification and distribution of ice particles in MBL clouds. An HSRL-2 phase mask was developed to differentiate depolarization from multiple scattering in water clouds versus from irregular ice particles and was compared with estimates of the ice and liquid water extinction fractions using in situ measurements from the FCDP and 2D-S probes (Crosbie et al. 2025). HSRL-2 vertically resolved cloudy regions with a linear depolarization ratio between the upper limit for multiple scattering and typical levels for ice (Burton et al. 2012) were assigned a mixed-phase classification. An example is shown in Fig. 8 from the morning flight on 9 December 2021 (RF 97) from NASA LaRC to Providence, Rhode Island. In this example, in situ ice extinction fractions greater than 1% were classified as mixed, while those above 90% were classified as ice and the frequency of each class is shown on the left side of the track for five temporal blocks in Fig. 8a. The equivalent frequency of each HSRL-2 class is shown on the right of the track and mimics the increase in mixed phase and ice occurrence in the second half of the northeast bound leg in an area where cloud heights peak and subsequently become more variable. The time–height cross section associated with this region is shown in detail (Fig. 8b) together with the coincident in situ extinction fraction time series (Fig. 8c) and captures the different regions of the cloud system penetrated by the Falcon. Prior to 1425 UTC, mixed-phase conditions were confirmed, while the comparison around 1430 UTC highlights a challenge with underidentifying ice under an opaque liquid-dominant cloud top and may explain part of the HSRL-2 underestimate near 68°W (Fig. 8a). Elsewhere, a small apparent false-positive mixed-phase classification cannot be further investigated without being able to interrogate the phase of smaller cloud particles than is possible with the 2D-S (~30 μm).

Other studies used HSRL-2 and/or RSP data to study aerosol properties. In a series of two studies (Siu et al. 2024a,b), the performance of RSP and HSRL-2 was evaluated using an established method called triple collocation (Stoffelen 1998). The lack of a suitable reference dataset over the remote ocean was overcome by introducing one more independent dataset (i.e., MODIS). HSRL-2 provided the best retrieval over the study region. Schlosser et al. (2022) leveraged the joint deployment of the RSP and HSRL-2 on the King Air to introduce a new technique for retrieving vertically resolved aerosol number density N_a. The method relies on taking a ratio between vertically resolved aerosol extinction coefficients (HSRL-2) and

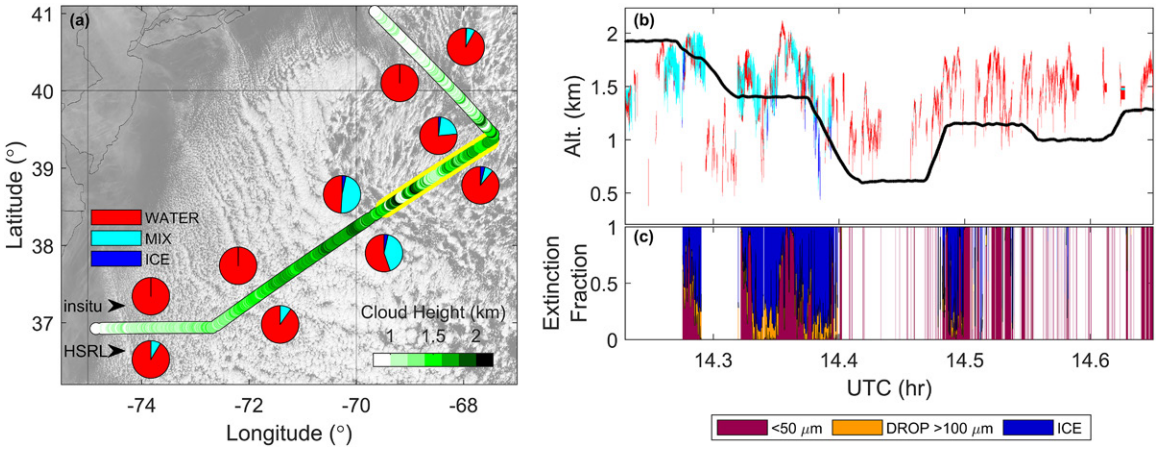

Fig. 8. (a) Comparison of HSRL-2 cloud-phase classification with in situ cloud probes during RF 97 on 9 Dec 2021. (b) Time–altitude cross section of the HSRL-2 phase classification during a flight segment (location shown in yellow in (a) and (c) the coincident extinction fraction attributed to small droplets measured by the FCDP in addition to large droplets and ice particles measured by the 2D-S.

fine-mode column-averaged aerosol extinction cross section (RSP). To guide combined polarimeter and lidar studies, a new lookup table was introduced to expedite single-scattering cloud calculations for water droplets, with its effectiveness demonstrated by comparing HSRL-2 data with in situ cloud measurements on the Falcon (Chemyakin et al. 2023). van Diedenhoven et al. (2022) introduced methods to infer aerosol volume water fraction, soluble fraction, and fine-mode dry size distributions from RSP data.

The joint deployment of the HSRL-2 and the NSF National Center for Atmospheric Research (NCAR) Airborne Vertical Atmosphere Profiling System (AVAPS) on the King Air allowed for rigorous assessments of a new HSRL-2 ocean surface wind speed product (Dmitrovic et al. 2024) and quantification of both the mixed layer height and planetary boundary layer height (Xu et al. 2024). As clouds above aircraft with nadir-viewing passive remote sensors can contaminate measurements, Nied et al. (2023) developed the cloud detection neural network (CDNN) based on forward-viewing or zenith-viewing aircraft camera data to identify such scenes to improve data analysis studies.

Two additional studies used ACTIVATE data to study aerosol retrievals performed using data from the CALIOP sensor. The combination of in situ Falcon aerosol size and composition data with dropsonde and HSRL-2 profiles of aerosol backscattering, extinction, and depolarization helped to characterize the enhanced aerosol depolarization produced by nonspherical sea salt particles (Ferrare et al. 2023). An important implication of this study is that the CALIOP v4.51 aerosol retrievals likely misclassified these marine aerosols as dust or dusty mix aerosols, which leads to overestimates (~40%–50%) in assumed lidar ratios and consequently aerosol extinction and AOD. Ryan et al. (2024) used HSRL-2 measurements collected during ACTIVATE and other field missions to evaluate AOD (532 nm) derived from the CALIOP Ocean Derived Column Optical Depth (ODCOD) algorithm. This method uses the CALIOP integrated attenuated backscatter from the ocean surface, together with collocated wind speed estimates from Modern-Era Retrospective Analysis for Research and Applications, version 2 (MERRA-2), to derive total full column optical depths of atmospheric particulates. ODCOD retrievals provide an estimate of total column optical depth contributed by all particulates in the column without relying on the detection of atmospheric layers done in the standard CALIOP retrieval algorithm. ODCOD and HSRL-2 AOD values agreed well with median ± median absolute deviation of 0.009 ± 0.043 (ODCOD higher).

7. Integration of modeling with observations

ACTIVATE's conception involved a strong research focus using a hierarchy of modeling tools, including large-eddy simulation (LES), cloud-resolving modeling (CRM), and single-column modeling (SCM), to simulate MBL clouds and understand ACI along with relevant thermodynamical and dynamical processes such as entrainment and turbulence. The hierarchical modeling framework, as illustrated in Fig. S2, integrates observational data from the ACTIVATE process study cases and meteorological reanalysis (such as ERA5 and MERRA-2) to advance process-level understanding of ACI and to quantify cloud susceptibility to aerosol perturbations (Tang et al. 2024). Long-term SCM simulations can take a further step to evaluate physics parameterizations and dynamical feedback related to ACI in Earth system models (ESMs) using the unprecedented number of statistical survey flights. The high data volume gathered during ACTIVATE is conducive toward ACI evaluation in ESMs, especially for features exhibiting a wide dynamic range of values across seasons. This was demonstrated early on during ACTIVATE by Brunke et al. (2022), who showed that turbulence simulated by two Energy Exascale ESM Atmosphere Model, version 2 (EAMv2), and Community Atmosphere Model, version 6 (CAM6), was too weak compared to observations. The impact of such turbulence bias on the N_a–N_d relationship has also been confirmed by Tang et al. (2024) in the EAMv2 SCM simulations.

An important feature of the northwest Atlantic is the Gulf Stream featuring warm SSTs that influence cloud properties especially in wintertime behind cold fronts. To simulate clouds in such conditions, it is important to use accurate initialization data and forcings that are often from coarse-resolution reanalysis data. Seethala et al. (2021) showed that reanalyses (ERA5 and MERRA-2) overly broaden the Gulf Stream compared to satellite depictions at 10-km spatial resolution, but are nevertheless adequate for the purpose of initializing higher-resolution modeling of the CAO clouds, as demonstrated in our LES, CRM, and SCM studies (Chen et al. 2022; Li et al. 2023, 2022; Tang et al. 2024).

ACTIVATE provides observations to constrain and evaluate hierarchical LES, CRM, and SCM simulations. LES was evaluated for how well it could capture cloud processes and MBL turbulence for two CAO case studies (28 February and 1 March 2020) (Li et al. 2022). First, an intercomparison made between dropsonde data and reanalysis for vertical velocity revealed reasonable agreement, providing confidence to use time-varying large-scale forcing (divergence and advective tendencies) profiles from ERA5 to drive the SCM and the Weather Research and Forecasting Model in the idealized LES mode (WRF-LES). With initial conditions, surface fluxes, and large-scale forcings from ERA5 (validated by ACTIVATE flight data including dropsondes) as the input, WRF-LES produced similar MBL meteorological states and cloud LWP for the two CAO cases to the ERA5 and flight measurements. Sensitivity analysis showed that divergence was pivotal in suppressing MBL evolution, while surface heat fluxes were more important for LWP. That study paved the way for continued analysis into ACI in these two cases. Initialized by measured aerosol size distributions and hygroscopicity (kappa) derived from aerosol mass spectrometer (AMS) composition data, LES reproduced vertical profiles of microphysical properties (LWC, N_d, and r_{eff}) when compared to in situ measurements (Li et al. 2023). Compared to the LES and observations, ERA5 was more successful than MERRA-2 in simulating the transient behavior of LWP and cloud fraction in the CAO cases, while both CRM and SCM simulate a lower LWP likely due to their weaker turbulence strength (Tang et al. 2024).

Li et al. (2024a) conducted an analogous LES analysis of ACI for two summertime precipitating cases on 2 June (cleaner, more precipitation) and 7 June (more polluted, less precipitation) 2021. The significant spatial heterogeneity of humidity, the deep weakly forced MBL, and their quickly evolving behavior on these two flights made the clouds challenging to simulate. While the WRF-LES was able to reproduce some features of these two cases such as reasonable cloud properties (LWC, N_d, and r_{eff}) and ACI metrics for the summer season (as in Fig. 5), they showed that quantifying precipitation susceptibility in such clouds is challenging (in contrast to stratocumulus clouds) as the relation between N_a and precipitation rate is strongly nonlinear. Li et al. (2024a) showed that the aerosol-induced LWP adjustment was governed more by precipitation feedback for both cases, in contrast to entrainment feedback, and emphasized the need for a better understanding of shallow convection and its dynamic environment as well as their interplay with cloud microphysics.

Unlike the LES and SCM tools, regional CRM can take boundary and surface forcing conditions from meteorological analysis/reanalysis products as input data to simulate more realistic spatial heterogeneity in atmospheric states and mesoscale circulation. Chen et al. (2022) used the WRF-CRM to study the morphology of the postfrontal clouds for the CAO case on 1 March 2020 and demonstrated the sensitivity of cloud roll structures, comparable to satellite-observed cloud scenes, to MBL wind shear and underlying SST, which the LES and SCM are incapable of representing. Tang et al. (2024) compared cloud formation and evolution in LES, CRM, and SCM for the same CAO case and showed similarities and unique differences in clouds, large-scale forcing, and surface fluxes in the CRM, indicating an important role of dynamical and thermodynamical feedback in ACI that also affects ambient meteorological conditions. LES and CRM together can inform SCM of the roles of resolved turbulent eddies,

cloud microphysics, and mesoscale circulation in characterizing clouds, boundary layer meteorology, and ACI.

8. Outreach and open data

A significant push was made among NASA EVS-3 missions to promote data usage with the incorporation of open data workshops. These served the purpose of reaching a broader audience not involved in conducting the campaign to showcase collected data and how it can be used. ACTIVATE held four formal open data workshops in October 2021 and in November 2022, 2023, and 2024. The first was conducted virtually because the COVID-19 pandemic prevented an in-person meeting. The latter three open workshops were in the form of ACTIVATE's annual science team meetings, which were made open to the public. These meetings had dedicated sessions that also focused on how the ACTIVATE datasets can be used.

Separately, the science team held more open data workshops for anyone interested to learn how to access and visualize ACTIVATE's airborne data. These virtual webinars held between July and September 2022 covered the science motivation of ACTIVATE and included interactive lessons to expose participants to Python. The webinars aimed to motivate the study of ACI and the importance of airborne measurements as well as the use of the Google Colaboratory (Google Colab) environment to examine atmospheric properties derived from both in situ and remote sensing products. These webinars were presented to high schools around the world, community college teachers, and those already in the ACI research community. Workshops were advertised broadly via email, social media, and various other online platforms. Recordings and slides are available (https://asdc.larc.nasa.gov/news/activate-data-webinar-materials).

A strength of ACTIVATE was the engagement of early career researchers in the team in conducting outreach, even in the midst of the COVID-19 pandemic when in-person contact was challenging. Ten graduate students hosted virtual sessions with middle and high school students in both the United States and other countries to teach them about ACTIVATE and NASA airborne science. Also, the ACTIVATE team extensively engaged students at various levels during the June 2022 deployment based in Bermuda with multiple outreach events in the aircraft hangar to teach students and their teachers about airborne science and ACI. Notable was the engagement with students (e.g., from 10-yr olds to graduate student level) and teachers from the Bermuda Institute of Ocean Sciences, Saltus Grammar School, Warwick Academy, and Victor Scott Primary. Two undergraduate interns were hired by ACTIVATE through the NASA Office of STEM Engagement to develop a neural network–based algorithm to produce cloud mask products for the airborne cameras on the King Air and Falcon aircraft. They published a paper on this method (Nied et al. 2023), successfully graduated, and are pursuing a Ph.D. in physics and atmospheric science.

Effort has been placed in data descriptor reports to summarize all details of not just the full ACTIVATE campaign (Sorooshian et al. 2023) but also individual datasets such as dropsondes (Vömel et al. 2023) and CCN and N_d (Sanchez et al. 2023). Open access code was developed to assist data users with collocating data between different aircraft (Schlosser et al. 2024).

9. Looking ahead

ACTIVATE successfully executed an aircraft campaign using a statistically focused approach with two spatially coordinated aircraft to study ACI in a region with significant seasonal variability in weather states and aerosol sources. This campaign builds on similar objectives of many that came before (e.g., Fig. 1) and provides a framework and extensive dataset for future airborne expeditions with statistical sampling in mind to allow for robust calculations of processes dependent on meteorology. Recognizing the challenge of using airborne data by scientists who are not involved in field campaigns (e.g., climate and weather modelers),

we are currently attempting to develop gridded data (at 0.05° and 0.25°) from airborne measurements.

There are extensive opportunities to leverage the ACTIVATE dataset to expand on early results and for new lines of pursuit. For instance, we are currently using the comprehensive ACTIVATE data and the hierarchical modeling framework, with SCM simulations having been conducted for all 3 years of the campaign, to evaluate and improve cloud microphysics parameterizations and dynamical feedback related to ACI in full ESMs and further assess their impact on global ACI modeling. Also, ACTIVATE conducted underflights along six targeted Advanced Spaceborne Thermal Emission and Reflection Radiometer (ASTER) tracks. The high-resolution (15 m) ASTER data provide a unique opportunity to study clouds at much finer spatial scales than those typically captured by satellite retrievals. By integrating ACTIVATE's in situ and remote sensing measurements with satellite cloud observations and ASTER data, ongoing efforts aim to assess the impact of environmental mixing processes—such as lateral cloud–ambient interactions and cloud-top entrainment—on cloud properties, while also identifying potential retrieval artifacts in conventional satellite cloud retrieval methods.

While the ACTIVATE dataset is useful for studies at subseasonal and seasonal scales, it also can help constrain and validate models at the interannual scale. The large number of ACTIVATE statistical survey flights enables the creation of rich and user-friendly datasets for advanced data science and machine learning methods. ACTIVATE's high data volume is uniquely valuable for this purpose, where repeated and consistent sampling of atmospheric phenomena is key to developing skillful and reliable models (e.g., Butler et al. 2025; Li et al. 2024b; Redemann and Gao 2024). Intercomparison of model simulations (e.g., LES with Lagrangian microphysics) based on ACTIVATE process study cases can be valuable for further process-level understanding and parameterization of ACI. By combining ACTIVATE data with improved CRM simulations, there are ongoing efforts aiming to understand the impact of Gulf Stream variations on the morphological transitioning of postfrontal clouds. More broadly, ACTIVATE's many postfrontal flights provide a uniquely robust dataset for the evaluation and development of key components in Earth system models. Relatively polluted clear sky conditions that were frequently sampled upwind of postfrontal clouds support the detailed study of aerosol schemes that predict aerosol type, mass, and number, while strong macro/microphysical gradients in the downwind cloud properties support the examination of interactions between cloud and aerosol processes. The adoption of a quasi-Lagrangian analysis and modeling approach to postfrontal ACTIVATE flights (Tornow et al. 2025) will particularly help the latter by providing multiple cases that span a progression of ACI during marine boundary layer transport. Such case studies collectively are suitable for model intercomparison projects and provide a strong foundation for model development via both LES with periodic boundary conditions and ESMs in SCM mode (Neggers 2015; Pithan et al. 2018).

Acknowledgments. The work was funded by ACTIVATE, a NASA Earth Venture Suborbital-3 (EVS-3) investigation funded by NASA's Earth Science Division and managed through the Earth System Science Pathfinder Program Office. The authors thank pilots and aircraft maintenance personnel of NASA Langley Research Services Directorate for the successful execution of ACTIVATE flights. University of Arizona investigators were supported by the National Aeronautics and Space Administration Grant 80NSSC19K0442. C. V. and S. K. thank funding by the Deutsche Forschungsgemeinschaft (DFG, German Research Foundation)—TRR 301—Project ID 428312742 and SPP 1294 HALO under Contract VO 1504/7-1. National Institute of Aerospace investigators were supported by NASA Grant 80NSSC19K0389. J. S. S. was supported by an appointment to the NASA Postdoctoral Program at NASA Langley Research Center, administered by Oak Ridge Associated Universities under contract

with NASA. The University of Miami acknowledges financial support through NASA Grant 80NSSC19K0390. Pacific Northwest National Laboratory (PNNL) investigators were supported by the NASA Grants NNL19OB08I and NNL24OB07A. PNNL is operated for DOE by Battelle Memorial Institute under Contract DE-AC05-76RLO1830. GEOS-FP weather and aerosol forecasts were obtained from the Global Modeling and Assimilation Office (GMAO) at the NASA Goddard Space Flight Center. The NASA Center for Climate Simulation (NCCS) provided supercomputing resources for GEOS-FP forecast processing and GEOS-Chem model simulations. We thank Ann Fridlind for helpful comments. The authors acknowledge Andreas Dörnbrack and Sonja Gisinger for forecasting support during ACTIVATE. We dedicate this work to the memory of both Claire Robinson and Rodrigo Delgado-Urzúa.

Data availability statement. The ACTIVATE data are publicly archived on NASA's Atmospheric Science Data Center (ASDC) Distributed Active Archive Center (DAAC; https://doi.org/10.5067/SUBORBITAL/ACTIVATE/DATA001) and are accessible via https://asdc.larc.nasa.gov/project/ACTIVATE.

References

Aldhaif, A. M., D. H. Lopez, H. Dadashazar, and A. Sorooshian, 2020: Sources, frequency, and chemical nature of dust events impacting the United States East Coast. *Atmos. Environ.*, **231**, 117456, https://doi.org/10.1016/j.atmosenv.2020.117456.

——, ——, ——, D. Painemal, A. J. Peters, and A. Sorooshian, 2021: An aerosol climatology and implications for clouds at a remote marine site: Case study over Bermuda. *J. Geophys. Res. Atmos.*, **126**, e2020JD034038, https://doi.org/10.1029/2020jd034038.

Andreae, M. O., 2009: Correlation between cloud condensation nuclei concentration and aerosol optical thickness in remote and polluted regions. *Atmos. Chem. Phys.*, **9**, 543–556, https://doi.org/10.5194/acp-9-543-2009.

Angevine, W. M., M. Trainer, S. A. McKeen, and C. M. Berkowitz, 1996: Mesoscale meteorology of the New England coast, Gulf of Maine, and Nova Scotia: Overview. *J. Geophys. Res.*, **101**, 28 893–28 901, https://doi.org/10.1029/95JD03271.

Bellouin, N., and Coauthors, 2020: Bounding global aerosol radiative forcing of climate change. *Rev. Geophys.*, **58**, e2019RG000660, https://doi.org/10.1029/2019RG000660.

Bock, L., and Coauthors, 2020: Quantifying progress across different CMIP phases with the ESMValTool. *J. Geophys. Res. Atmos.*, **125**, e2019JD032321, https://doi.org/10.1029/2019JD032321.

Bony, S., and J.-L. Dufresne, 2005: Marine boundary layer clouds at the heart of tropical cloud feedback uncertainties in climate models. *Geophys. Res. Lett.*, **32**, L20806, https://doi.org/10.1029/2005GL023851.

Bretherton, C. S., 2015: Insights into low-latitude cloud feedbacks from high-resolution models. *Philos. Trans. Roy. Soc.*, **A373**, 20140415, https://doi.org/10.1098/rsta.2014.0415.

Brunke, M. A., and Coauthors, 2022: Aircraft observations of turbulence in cloudy and cloud-free boundary layers over the western North Atlantic Ocean from ACTIVATE and implications for the Earth system model evaluation and development. *J. Geophys. Res. Atmos.*, **127**, e2022JD036480, https://doi.org/10.1029/2022JD036480.

Burton, S. P., and Coauthors, 2012: Aerosol classification using airborne high spectral resolution lidar measurements—Methodology and examples. *Atmos. Meas. Tech.*, **5**, 73–98, https://doi.org/10.5194/amt-5-73-2012.

Butler, K. M., and Coauthors, 2025: Investigating reduced-dimensional variability in aircraft-observed aerosol–cloud parameters. *Environ. Data Sci.*, **4**, e27, https://doi.org/10.1017/eds.2025.17.

Chemyakin, E., and Coauthors, 2023: Efficient single-scattering look-up table for lidar and polarimeter water cloud studies. *Opt. Lett.*, **48**, 13–16, https://doi.org/10.1364/OL.474282.

Chen, J., H. Wang, X. Li, D. Painemal, A. Sorooshian, K. L. Thornhill, C. Robinson, and T. Shingler, 2022: Impact of meteorological factors on the mesoscale morphology of cloud streets during a cold-air outbreak over the western North Atlantic. *J. Atmos. Sci.*, **79**, 2863–2879, https://doi.org/10.1175/JAS-D-22-0034.1.

Choudhury, G., and M. Tesche, 2023: A first global height-resolved cloud condensation nuclei data set derived from spaceborne lidar measurements. *Earth Syst. Sci. Data*, **15**, 3747–3760, https://doi.org/10.5194/essd-15-3747-2023.

Corral, A. F., H. Dadashazar, C. Stahl, E.-L. Edwards, P. Zuidema, and A. Sorooshian, 2020: Source apportionment of aerosol at a coastal site and relationships with precipitation chemistry: A case study over the southeast United States. *Atmosphere*, **11**, 1212, https://doi.org/10.3390/atmos11111212.

——, and Coauthors, 2021: An overview of atmospheric features over the western North Atlantic Ocean and North American East Coast – Part 1: Analysis of aerosols, gases, and wet deposition chemistry. *J. Geophys. Res. Atmos.*, **126**, e2020JD032592, https://doi.org/10.1029/2020jd032592.

——, and Coauthors, 2022a: Dimethylamine in cloud water: A case study over the northwest Atlantic Ocean. *Environ. Sci.: Atmos.*, **2**, 1534–1550, https://doi.org/10.1039/D2EA00117A.

——, and Coauthors, 2022b: Cold air outbreaks promote new particle formation off the U.S. East Coast. *Geophys. Res. Lett.*, **49**, e2021GL096073, https://doi.org/10.1029/2021GL096073.

Crosbie, E., and Coauthors, 2024: Measurement report: Cloud and environmental properties associated with aggregated shallow marine cumulus and cumulus congestus. *Atmos. Chem. Phys.*, **24**, 6123–6152, https://doi.org/10.5194/acp-24-6123-2024.

——, and Coauthors, 2025: A method to retrieve mixed-phase cloud vertical structure from airborne lidar. *Atmos. Meas. Tech.*, **18**, 2639–2658, https://doi.org/10.5194/amt-18-2639-2025.

Cutler, L., M. A. Brunke, and X. Zeng, 2022: Re-evaluation of low cloud amount relationships with lower-tropospheric stability and estimated inversion strength. *Geophys. Res. Lett.*, **49**, e2022GL098137, https://doi.org/10.1029/2022GL098137.

Dadashazar, H., and Coauthors, 2021a: Aerosol responses to precipitation along North American air trajectories arriving at Bermuda. *Atmos. Chem. Phys.*, **21**, 16 121–16 141, https://doi.org/10.5194/acp-21-16121-2021.

——, and Coauthors, 2021b: Cloud drop number concentrations over the western North Atlantic Ocean: Seasonal cycle, aerosol interrelationships, and other influential factors. *Atmos. Chem. Phys.*, **21**, 10 499–10 526, https://doi.org/10.5194/acp-21-10499-2021.

——, and Coauthors, 2022: Organic enrichment in droplet residual particles relative to out of cloud over the northwestern Atlantic: Analysis of airborne ACTIVATE data. *Atmos. Chem. Phys.*, **22**, 13 897–13 913, https://doi.org/10.5194/acp-22-13897-2022.

Davis, R. E., B. P. Hayden, D. A. Gay, W. L. Phillips, and G. V. Jones, 1997: The North Atlantic subtropical anticyclone. *J. Climate*, **10**, 728–744, https://doi.org/10.1175/1520-0442(1997)010<0728:TNASA>2.0.CO;2.

Dmitrovic, S., and Coauthors, 2024: High Spectral Resolution Lidar—Generation 2 (HSRL-2) retrievals of ocean surface wind speed: Methodology and evaluation. *Atmos. Meas. Tech.*, **17**, 3515–3532, https://doi.org/10.5194/amt-17-3515-2024.

Duong, H. T., A. Sorooshian, and G. Feingold, 2011: Investigating potential biases in observed and modeled metrics of aerosol-cloud-precipitation interactions. *Atmos. Chem. Phys.*, **11**, 4027–4037, https://doi.org/10.5194/acp-11-4027-2011.

Edwards, E.-L., A. F. Corral, H. Dadashazar, A. E. Barkley, C. J. Gaston, P. Zuidema, and A. Sorooshian, 2021: Impact of various air mass types on cloud condensation nuclei concentrations along coastal southeast Florida. *Atmos. Environ.*, **254**, 118371, https://doi.org/10.1016/j.atmosenv.2021.118371.

——, and Coauthors, 2024: Sea salt reactivity over the northwest Atlantic: An in-depth look using the airborne ACTIVATE dataset. *Atmos. Chem. Phys.*, **24**, 3349–3378, https://doi.org/10.5194/acp-24-3349-2024.

Feingold, G., L. A. Remer, J. Ramaprasad, and Y. J. Kaufman, 2001: Analysis of smoke impact on clouds in Brazilian biomass burning regions: An extension of Twomey's approach. *J. Geophys. Res.*, **106**, 22 907–22 922, https://doi.org/10.1029/2001JD000732.

Ferrare, R., and Coauthors, 2023: Airborne HSRL-2 measurements of elevated aerosol depolarization associated with non-spherical sea salt. *Front. Remote Sens.*, **4**, 1143944, https://doi.org/10.3389/frsen.2023.1143944.

Gassó, S., and D. A. Hegg, 2003: On the retrieval of columnar aerosol mass and CCN concentration by MODIS. *J. Geophys. Res.*, **108**, 4010, https://doi.org/10.1029/2002JD002382.

Ghan, S. J., and D. R. Collins, 2004: Use of in situ data to test a Raman lidar–based cloud condensation nuclei remote sensing method. *J. Atmos. Oceanic Technol.*, **21**, 387–394, https://doi.org/10.1175/1520-0426(2004)021<0387:UOISDT>2.0.CO;2.

——, and Coauthors, 2006: Use of in situ cloud condensation nuclei, extinction, and aerosol size distribution measurements to test a method for retrieving cloud condensation nuclei profiles from surface measurements. *J. Geophys. Res.*, **111**, D05S10, https://doi.org/10.1029/2004JD005752.

Gonzalez, M. E., and Coauthors, 2022: Relationships between supermicrometer particle concentrations and cloud water sea salt and dust concentrations: Analysis of MONARC and ACTIVATE data. *Environ. Sci.: Atmos.*, **2**, 738–752, https://doi.org/10.1039/D2EA00049K.

Gryspeerdt, E., A. C. Povey, R. G. Grainger, O. Hasekamp, N. C. Hsu, J. P. Mulcahy, A. M. Sayer, and A. Sorooshian, 2023: Uncertainty in aerosol–cloud radiative forcing is driven by clean conditions. *Atmos. Chem. Phys.*, **23**, 4115–4122, https://doi.org/10.5194/acp-23-4115-2023.

Hair, J., and Coauthors, 2024: Vertical profiles of cloud extinction and cloud top droplet number concentration in warm clouds derived from airborne lidar and polarimeter measurements. *31st Int. Laser Radar Conf.*, Landshut, Germany, DLR.

Hilario, M. R. A., and Coauthors, 2021: Particulate oxalate-to-sulfate ratio as an aqueous processing marker: Similarity across field campaigns and limitations. *Geophys. Res. Lett.*, **48**, e2021GL096520, https://doi.org/10.1029/2021gl096520.

Hurrell, J. W., 1995: Decadal trends in the North Atlantic Oscillation: Regional temperatures and precipitation. *Science*, **269**, 676–679, https://doi.org/10.1126/science.269.5224.676.

Kapustin, V. N., A. D. Clarke, Y. Shinozuka, S. Howell, V. Brekhovskikh, T. Nakajima, and A. Higurashi, 2006: On the determination of a cloud condensation nuclei from satellite: Challenges and possibilities. *J. Geophys. Res.*, **111**, D04202, https://doi.org/10.1029/2004JD005527.

Kirschler, S., and Coauthors, 2022: Seasonal updraft speeds change cloud droplet number concentrations in low-level clouds over the western North Atlantic. *Atmos. Chem. Phys.*, **22**, 8299–8319, https://doi.org/10.5194/acp-22-8299-2022.

——, and Coauthors, 2023: Overview and statistical analysis of boundary layer clouds and precipitation over the western North Atlantic Ocean. *Atmos. Chem. Phys.*, **23**, 10731–10750, https://doi.org/10.5194/acp-23-10731-2023.

Lamb, P. J., and R. A. Peppler, 1987: North Atlantic Oscillation: Concept and an application. *Bull. Amer. Meteor. Soc.*, **68**, 1218–1225, https://doi.org/10.1175/1520-0477(1987)068<1218:NAOCAA>2.0.CO;2.

Landsea, C. W., and J. L. Franklin, 2013: Atlantic hurricane database uncertainty and presentation of a new database format. *Mon. Wea. Rev.*, **141**, 3576–3592, https://doi.org/10.1175/MWR-D-12-00254.1.

Li, X.-Y., and Coauthors, 2022: Large-eddy simulations of marine boundary layer clouds associated with cold-air outbreaks during the ACTIVATE campaign. Part I: Case setup and sensitivities to large-scale forcings. *J. Atmos. Sci.*, **79**, 73–100, https://doi.org/10.1175/JAS-D-21-0123.1.

——, and Coauthors, 2023: Large-eddy simulations of marine boundary layer clouds associated with cold-air outbreaks during the ACTIVATE campaign. Part II: Aerosol–meteorology–cloud interaction. *J. Atmos. Sci.*, **80**, 1025–1045, https://doi.org/10.1175/JAS-D-21-0324.1.

——, and Coauthors, 2024a: Process modeling of aerosol-cloud interaction in summertime precipitating shallow cumulus over the western North Atlantic. *J. Geophys. Res. Atmos.*, **129**, e2023JD039489, https://doi.org/10.1029/2023JD039489.

——, H. Wang, T. C. Chakraborty, A. Sorooshian, L. D. Ziemba, C. Voigt, K. L. Thornhill, and E. Yuan, 2024b: On the prediction of aerosol-cloud interactions within a data-driven framework. *Geophys. Res. Lett.*, **51**, e2024GL110757, https://doi.org/10.1029/2024GL110757.

Liu, H., and Coauthors, 2025: Tropospheric aerosols over the western North Atlantic Ocean during the winter and summer deployments of ACTIVATE 2020: Life cycle, transport, and distribution. *Atmos. Chem. Phys.*, **25**, 2087–2121, https://doi.org/10.5194/acp-25-2087-2025.

Lucchesi, R., 2018: File specification for GEOS FP. GMAO Office Note 4 (version 1.2). 62 pp., https://gmao.gsfc.nasa.gov/pubs/docs/Lucchesi1203.pdf.

Ma, L., H. Dadashazar, M. R. A. Hilario, M. O. Cambaliza, G. R. Lorenzo, J. B. Simpas, P. Nguyen, and A. Sorooshian, 2021: Contrasting wet deposition composition between three diverse islands and coastal North American sites. *Atmos. Environ.*, **244**, 117919, https://doi.org/10.1016/j.atmosenv.2020.117919.

Mardi, A. H., H. Dadashazar, D. Painemal, T. Shingler, S. T. Seaman, M. A. Fenn, C. A. Hostetler, and A. Sorooshian, 2021: Biomass burning over the United States East Coast and western North Atlantic Ocean: Implications for clouds and air quality. *J. Geophys. Res. Atmos.*, **126**, e2021JD034916, https://doi.org/10.1029/2021jd034916.

McComiskey, A., and G. Feingold, 2008: Quantifying error in the radiative forcing of the first aerosol indirect effect. *Geophys. Res. Lett.*, **35**, L02810, https://doi.org/10.1029/2007GL032667.

——, and ——, 2012: The scale problem in quantifying aerosol indirect effects. *Atmos. Chem. Phys.*, **12**, 1031–1049, https://doi.org/10.5194/acp-12-1031-2012.

——, ——, A. S. Frisch, D. D. Turner, M. A. Miller, J. C. Chiu, Q. Min, and J. A. Ogren, 2009: An assessment of aerosol-cloud interactions in marine stratus clouds based on surface remote sensing. *J. Geophys. Res.*, **114**, D09203, https://doi.org/10.1029/2008JD011006.

Minobe, S., A. Kuwano-Yoshida, N. Komori, S. P. Xie, and R. J. Small, 2008: Influence of the Gulf Stream on the troposphere. *Nature*, **452**, 206–209, https://doi.org/10.1038/nature06690.

Molod, A., L. Takacs, M. J. Suarez, J. Bacmeister, I. S. Song, and A. Eichmann, 2012: The GEOS-5 atmospheric general circulation model: Mean climate and development from MERRA to Fortuna. NASA/TM-2012-104606, Vol. 28, 124 pp., https://gmao.gsfc.nasa.gov/pubs/docs/Molod484.pdf.

NASEM, 2018: *Thriving on Our Changing Planet: A Decadal Strategy for Earth Observation from Space.* The National Academies Press, 716 pp.

Neggers, R. A. J., 2015: Attributing the behavior of low-level clouds in large-scale models to subgrid-scale parameterizations. *J. Adv. Model. Earth Syst.*, **7**, 2029–2043, https://doi.org/10.1002/2015MS000503.

Nied, J., and Coauthors, 2023: A cloud detection neural network for above-aircraft clouds using airborne cameras. *Front. Remote Sens.*, **4**, 1118745, https://doi.org/10.3389/frsen.2023.1118745.

Painemal, D., and P. Zuidema, 2013: The first aerosol indirect effect quantified through airborne remote sensing during VOCALS-REx. *Atmos. Chem. Phys.*, **13**, 917–931, https://doi.org/10.5194/acp-13-917-2013.

——, and Coauthors, 2021: An overview of atmospheric features over the western North Atlantic Ocean and North American East Coast—Part 2: Circulation, boundary layer, and clouds. *J. Geophys. Res. Atmos.*, **126**, e2020JD033423, https://doi.org/10.1029/2020JD033423.

——, and Coauthors, 2023: Wintertime synoptic patterns of midlatitude boundary layer clouds over the western North Atlantic: Climatology and insights from in situ ACTIVATE observations. *J. Geophys. Res. Atmos.*, **128**, e2022JD037725, https://doi.org/10.1029/2022JD037725.

Park, J. M., A. C. McComiskey, D. Painemal, and W. L. Smith Jr., 2024: Long-term trends in aerosols, low clouds, and large-scale meteorology over the western North Atlantic from 2003 to 2020. *J. Geophys. Res. Atmos.*, **129**, e2023JD039592, https://doi.org/10.1029/2023JD039592.

Pithan, F., and Coauthors, 2018: Role of air-mass transformations in exchange between the Arctic and mid-latitudes. *Nat. Geosci.*, **11**, 805–812, https://doi.org/10.1038/s41561-018-0234-1.

Redemann, J., and L. Gao, 2024: A machine learning paradigm for necessary observations to reduce uncertainties in aerosol climate forcing. *Nat. Commun.*, **15**, 8343, https://doi.org/10.1038/s41467-024-52747-y.

Rémillard, J., and G. Tselioudis, 2015: Cloud regime variability over the Azores and its application to climate model evaluation. *J. Climate*, **28**, 9707–9720, https://doi.org/10.1175/JCLI-D-15-0066.1.

Rienecker, M. M., and Coauthors, 2008: The GEOS-5 Data Assimilation System—Documentation of versions 5.0.1, 5.1.0, and 5.2.0. Tech. Memo. NASA/TM-2008-104606, Vol. 27, 118 pp., https://gmao.gsfc.nasa.gov/pubs/docs/Rienecker369.pdf.

Ryan, R. A., and Coauthors, 2024: Total column optical depths retrieved from CALIPSO lidar ocean surface backscatter. *Atmos. Meas. Tech.*, **17**, 6517–6545, https://doi.org/10.5194/amt-17-6517-2024.

Sanchez, K. J., and Coauthors, 2023: Multi-campaign ship and aircraft observations of marine cloud condensation nuclei and droplet concentrations. *Sci. Data*, **10**, 471, https://doi.org/10.1038/s41597-023-02372-z.

Schlosser, J. S., and Coauthors, 2022: Polarimeter + lidar–derived aerosol particle number concentration. *Front. Remote Sens.*, **3**, 885332, https://doi.org/10.3389/frsen.2022.885332.

——, and Coauthors, 2024: Maximizing the volume of collocated data from two coordinated suborbital platforms. *J. Atmos. Oceanic Technol.*, **41**, 189–201, https://doi.org/10.1175/JTECH-D-23-0001.1.

Seethala, C., and Coauthors, 2021: On assessing ERA5 and MERRA2 representations of cold-air outbreaks across the Gulf Stream. *Geophys. Res. Lett.*, **48**, e2021GL094364, https://doi.org/10.1029/2021gl094364.

——, and Coauthors, 2024: Microphysical evolution in mixed-phase mid-latitude marine cold-air outbreaks. *J. Atmos. Sci.*, **81**, 1725–1747, https://doi.org/10.1175/JAS-D-23-0203.1.

Sherwood, S. C., S. Bony, and J.-L. Dufresne, 2014: Spread in model climate sensitivity traced to atmospheric convective mixing. *Nature*, **505**, 37–42, https://doi.org/10.1038/nature12829.

Shinozuka, Y., and Coauthors, 2015: The relationship between cloud condensation nuclei (CCN) concentration and light extinction of dried particles: Indications of underlying aerosol processes and implications for satellite-based CCN estimates. *Atmos. Chem. Phys.*, **15**, 7585–7604, https://doi.org/10.5194/acp-15-7585-2015.

Siu, L. W., and Coauthors, 2024a: Summarizing multiple aspects of triple collocation analysis in a single diagram. *Front. Remote Sens.*, **5**, 1395442, https://doi.org/10.3389/frsen.2024.1395442.

——, and Coauthors, 2024b: Retrievals of aerosol optical depth over the western North Atlantic Ocean during ACTIVATE. *Atmos. Meas. Tech.*, **17**, 2739–2759, https://doi.org/10.5194/amt-17-2739-2024.

Soloff, C., and Coauthors, 2024: Bridging gas and aerosol properties between the northeastern US and Bermuda: Analysis of eight transit flights. *Atmos. Chem. Phys.*, **24**, 10 385–10 408, https://doi.org/10.5194/acp-24-10385-2024.

Sorooshian, A., and Coauthors, 2019: Aerosol–cloud–meteorology interaction airborne field investigations: Using lessons learned from the U.S. West Coast in the design of ACTIVATE off the U.S. East Coast. *Bull. Amer. Meteor. Soc.*, **100**, 1511–1528, https://doi.org/10.1175/BAMS-D-18-0100.1.

——, and Coauthors, 2020: Atmospheric research over the western North Atlantic Ocean region and North American East Coast: A review of past work and challenges ahead. *J. Geophys. Res. Atmos.*, **125**, e2019JD031626, https://doi.org/10.1029/2019jd031626.

——, and Coauthors, 2023: Spatially coordinated airborne data and complementary products for aerosol, gas, cloud, and meteorological studies: The NASA ACTIVATE dataset. *Earth Syst. Sci. Data*, **15**, 3419–3472, https://doi.org/10.5194/essd-15-3419-2023.

Stier, P., 2016: Limitations of passive remote sensing to constrain global cloud condensation nuclei. *Atmos. Chem. Phys.*, **16**, 6595–6607, https://doi.org/10.5194/acp-16-6595-2016.

Stoffelen, A., 1998: Toward the true near-surface wind speed: Error modeling and calibration using triple collocation. *J. Geophys. Res.*, **103**, 7755–7766, https://doi.org/10.1029/97JC03180.

Tang, S., and Coauthors, 2024: Understanding aerosol–cloud interactions using a single-column model for a cold-air outbreak case during the ACTIVATE campaign. *Atmos. Chem. Phys.*, **24**, 10 073–10 092, https://doi.org/10.5194/acp-24-10073-2024.

Tornow, F., A. S. Ackerman, and A. M. Fridlind, 2021: Preconditioning of overcast-to-broken cloud transitions by riming in marine cold air outbreaks. *Atmos. Chem. Phys.*, **21**, 12 049–12 067, https://doi.org/10.5194/acp-21-12049-2021.

——, and Coauthors, 2022: Dilution of boundary layer cloud condensation nucleus concentrations by free tropospheric entrainment during marine cold air outbreaks. *Geophys. Res. Lett.*, **49**, e2022GL098444, https://doi.org/10.1029/2022GL098444.

——, A. S. Ackerman, A. M. Fridlind, G. Tselioudis, B. Cairns, D. Painemal, and G. Elsaesser, 2023: On the impact of a dry intrusion driving cloud-regime transitions in a midlatitude cold-air outbreak. *J. Atmos. Sci.*, **80**, 2881–2896, https://doi.org/10.1175/JAS-D-23-0040.1.

——, and Coauthors, 2025: Measurement report: A survey of meteorological and cloud properties during ACTIVATE's postfrontal flights and their suitability for Lagrangian case studies. *Atmos. Chem. Phys.*, **25**, 5053–5074, https://doi.org/10.5194/acp-25-5053-2025.

van Diedenhoven, B., O. P. Hasekamp, B. Cairns, G. L. Schuster, S. Stamnes, M. Shook, and L. Ziemba, 2022: Remote sensing of aerosol water fraction, dry size distribution and soluble fraction using multi-angle, multi-spectral polarimetry. *Atmos. Meas. Tech.*, **15**, 7411–7434, https://doi.org/10.5194/amt-15-7411-2022.

Vömel, H., A. Sorooshian, C. Robinson, T. J. Shingler, K. L. Thornhill, and L. D. Ziemba, 2023: Dropsonde observations during the aerosol cloud meteorology interactions over the western Atlantic experiment. *Sci. Data*, **10**, 753, https://doi.org/10.1038/s41597-023-02647-5.

Xu, Y., J. Arevalo, A. Ouyed, and X. Zeng, 2022: Precipitation over the U.S. Coastal land/water using Gauge-Corrected Multi-Radar/Multi-Sensor system and three satellite products. *Remote Sens.*, **14**, 4557, https://doi.org/10.3390/rs14184557.

——, and Coauthors, 2024: Boundary layer structures over the northwest Atlantic derived from airborne high spectral resolution lidar and dropsonde measurements during the ACTIVATE campaign. *J. Geophys. Res. Atmos.*, **129**, e2023JD039878, https://doi.org/10.1029/2023JD039878.

Zelinka, M. D., T. A. Myers, D. T. McCoy, S. Po-Chedley, P. M. Caldwell, P. Ceppi, S. A. Klein, and K. E. Taylor, 2020: Causes of higher climate sensitivity in CMIP6 models. *Geophys. Res. Lett.*, **47**, e2019GL085782, https://doi.org/10.1029/2019GL085782.

Zuidema, P., C. Alvarez, S. J. Kramer, L. Custals, M. Izaguirre, P. Sealy, J. M. Prospero, and E. Blades, 2019: Is summer African dust arriving earlier to Barbados? The updated long-term in situ dust mass concentration time series from ragged point, Barbados, and Miami, Florida. *Bull. Amer. Meteor. Soc.*, **100**, 1981–1986, https://doi.org/10.1175/BAMS-D-18-0083.1.